UNIVERSITY OF SALERNO

Department of Civil Engineering

Ph.D. Thesis
in
Risk and Sustainability in Civil, Architectural and
Environmental Engineering Systems

Cycle XXXIII (2017-2020)

OPTIMIZATION OF WATER TREATMENT PROCESSES
USING COMPUTATIONAL FLUID DYNAMICS

Simone Coppola

Supervisor	**Ph.D. Coordinator**
Prof. Giacomo Viccione	*Prof. Fernando Fraternali*

Advisors
Ing. Alessandro Meda
Ing. Eliana Perucca

Acknowledgments

It's an immense pleasure to express my sincere and deepest sense of gratitude that I have had the opportunity of working under the guidance of my supervisor Prof. Giacomo Viccione, who thus I sincerely thank for guiding me throughout the this project by making me to understand the work and providing me with all the facilities necessary to complete the project successfully.

I'm also grateful to Eng. Alessandro Meda and Eng. Eliana Perucca, my advisors for providing me an evaluable experience during my internships respectively at BHU umwelttechnik Gmbh (Germany) and Ai engineering s.r.l. (Italy)

I finally would like to thank my parents and my sister, without you none of this would had been possible. Thank you for all your support, inspiration, encouragement and everything you have done for me.

Index

7

1. Introduction

The development of Computational Fluid Dynamics (CFD) started over 40 years ago, as attempt to numerically solve fluid engineering problems in different fields of application.

CFD application in the past involved the study of fluid flow for civil and industrial applications, heat and mass transfer problems in aeronautics, vehicle aerodynamics, chemical engineering, nuclear design and safety, ventilation and industrial design but, due to the lack of available numerical models for material properties, the results were not accurate.

The CFD is strictly related to the computing power of the calculators. For this reason, its development, proposal of new algorithms as well as the enhancement of the existing ones, is related to the calculation capacities. Today, a Personal Computer of common usage, is able to perform simulations using computing domains featuring very fine discretization, getting good and reliable results at a reasonable time cost. There are also some open access calculation codes that allow to speed up the simulation. There are many advantages using open-source software. In addition to being free to use and distribute, open-source software provides users the license to modify source code as-needed. Open-source CFD solvers are not different. Some of the most common include OpenFOAM, SU2, Palabos, Fire Dynamics Simulator, Aquagpu, Dualsphysics and MFIX. Among the mentioned softwares the leading for Computational Fluid Dynamics is OpenFOAM. Indeed, it contains multiple solvers that can be applied to different types of flow problems, and a continuous development of the program is made taking into account the users feedbacks.

The term CFD refers to numerical models, solving the hydrodynamics governed by the Navier-stokes equations. Versteeg & Malalasekera, 1995 defines CFD as: *The analysis of systems involving fluid flow, heat transfer and associated phenomena such as chemical reactions by means of computer-based simulation.*

In such applications the boundary conditions, geometry and material properties of any solid surfaces are known precisely and the code is applied to a closed system. Indeed, in the mentioned cases it may be possible to characterize the complete existing process mechanisms obtaining good experimental data for model validation. Considerable effort is expended in the creation of codes on topic like numerical analysis, turbulence modelling, grid generation and adaptive meshing. The tolerance errors of the solution is low, and for this reason the mentioned codes are predominantly used in a deterministic approach as alternatives to the laboratory experimentation

This branch of science serves industrial engineering applications well, and the techniques thus developed have considerable spin-off benefit in other disciplines such as environmental hydraulics.

The potential for using computer models to simulate industrial flows is obvious, deterministic methodology used in industrial applications and wastewater treatments is considered appropriate because are known: geometry, easily meshable surface, boundary conditions, rheology of flows and drag coefficients that vary in time and space as result of complex interactions between the material properties of the surface and the flow itself. To have a sufficient level of detail the CFD models adopt finite representations of time and space that may be very different to the time and space scales over which observations are obtained, it may actually be very difficult to measure those quantities predicted by a given code. Whilst the CFD models used to perform numerical experiments in wastewater treatment plants, require comparisons with real data to be validated.

The CFD wastewater treatment plants modellers should be concerned about the numerical techniques they use and about the quality of the numerical solutions they produce. Therefore, a more highly resolved model grids and greater levels of process inclusion will not lead to more physically realistic models.

The best strategy to avoid the uncertainties in wastewater CFD modelling is the errors research, quantification and reduction in order to minimize the difference between the calculate model and the real measured condition. The measured data available may be sparse and contain significant but poorly known errors that vary strongly in time and space.

The ability to deal with problems characterized by sparse and uncertain data where there may even be debate over the fundamental process mechanisms at work is a key part of scientific training in environmental engineering.

Application of CFD techniques to real-world environmental problems has increased sharply in the last decade due to an improving ability to deal with the uncertainties noted above.

The strength points of CFD model for the simulation of WWTP's are the ability to model complex processes where measurements can be hard to obtain, the power to test alternative configuration of the tank in order to identify design faults and obtain increased performance. This save time and costs because the system can be retrofitted in a mathematical model before taking any physical action, but a detailed knowledge of the overall functioning of process tanks is required.

Theoretically, due to the division of the computational domain into infinitely small meshes the resolution of the results should be unlimited, but it requires a high computational time, a computer software and hardware with high performance.

Generally, CFD models should be coupled with model calibration, and a proper validation. Since CFD models are complex, only experienced specialists that know the inside of the model will be capable of creating trustworthy results. Until now, only large companies or universities have been using CFD models in their work due to the expensive software and the necessity of highly trained personnel.

In this thesis a contribution toward understanding the capabilities of CFD tools in solving WWTP applications is made. In Chapter 2, is outlined an overview of CFD applications in WWTPs considering biological processes that take place in the active sludge systems. Considering that the aim of this study is to optimize the simulations processes (Chapter 3). The chapter 4 is basically dedicated to explain the computational part of the problem, all the used software (COMSOL Multiphysics) equations are explained. Then in the following chapters are treated some real cases

2. An overview of CFD in WWTPs

2.1 CFD models

In water and wastewater treatment, the key question is how to control the quality of water to an acceptable level before it is sent to the users or environment. The parameters for water quality can be broadly categorized as physical, chemical, and biological. Monitoring programs are in place in almost all treatment plants to measure water quality at various stages of the treatment process and to ensure compliance of the final product.

Computational fluid dynamics has become a reliable method for process analysis of fluid flows in many industries. It recently has become widely used for analysis of hydraulic problems in water and wastewater treatment (WWT) but still needs to find wider acceptance for analysis of physical, chemical and biological processes in WWT. There are substantial financial and risk drivers to conduct CFD for better wastewater design (Wicklein et al., 2016).

Units of treatment plants with CFD are increasingly being analysed, focusing on the development of papers on a specific treatment process and its unit. The purpose of the current chapter is to provide an overview of the state of the art of applying CFD focalizing on the aspects used in clean water and WWT processes. This thesis refers to general methods solving mainly hydrodynamics for computational domains in either two or three dimensions (2D or 3D).

The most studied sub processes in the CFD model, where the continuity mass and momentum equations (see Chapter 3) are applied, are the aeration process, the mixing process, micro biological processes and the sedimentation processes.

CFD deals with the simultaneous numerical solution of the momentum and continuity equations for fluid mechanics. Generally, CFD relies on partial differential equation that typically have no analytical solution, for this reason numerical schemes are required, and are being solved in a discretized fluid domain consisting of a mesh grid (mesh-based methods), elements (FE kind of methods) or points (meshless methods).

2.2 Biological processes (suspended growth)

The biological processes treated in activated sludge tanks have a broad range of functionality, including nutrient and carbon removal, pathogen destruction, and

removal of micro pollutants. They are dependent on multiphase contact and effective hydraulic fields. For this reason, the potential benefits offered by CFD, could be assessing hydraulic behaviour in the domain and the gas–liquid transfer related with biological functionality.

The focus on suspended growth systems has been in activated sludge basins. In activated sludge, among all the biological processes, the suspended growth system (flocculation) is largely studied

The flocculation process is caused by the induced mixing of the suspended solids, where the generated velocity gradients makes particles of biomass and other matter collide into larger aggregates. Since larger sludge flocs in general have a larger settling velocity than smaller ones, and the settling velocity is dependent on the sludge characteristics. Therefore, the floc size can be increased by the agitation of the fluid but due to the limitations in floc strength, the size will depend on the shear of the suspension. When the floc size is increased, the biomass is more easily separated from the water phase.

There isn't a dedicated procedure for the stream flow calculation that ensure the efficiency of the simulation. The most adopted methodology, that at the moment provides an acceptable efficiency, is the RANS closed by k-ε or k-ω turbulence model.

A first valid model of sedimentation by (Parker et al. 1971; Parker et al. 1972) estimated the factors that affect flocculation in activated sludge mixed liquors. This model proposed a simple model for floc breakup and agglomeration, based on the root mean velocity gradient, G term. The mentioned model has been used and validated by researchers many times. In contrast to this, (Ducoste et al. 1998) demonstrated that the floc breakup was controlled by the turbulence intensity.

Many flocculation models have been studied; the limit of these models is due to the incapacity to represent specifically the physical phenomenon. The flocculation is strictly related to fluid dynamics of the units where it occurs, therefore the phenomenon is represented through turbulence models. These models are affected by closure problem errors, the luck of accuracy imply that they can just represent the trend of phenomenon.

Secondary sedimentation would appear to have similar challenges as the primary sedimentation, but it's actually governed by some different mechanisms. Modelling goals are also directed by the multiple functions of final effluent clarification, activated sludge thickening, sludge storage and flocculation.

In the secondary sedimentation tank, the activated sludge is widely studied in CFD application for WWTP. A lot of study used a 2D simulation including a transport and settling processes, related to fluid flow in the tank, for solids concentration.

3. The aim of research

As mentioned before, the research is here carried out with reference to the complete hydrodynamic and process modelling in wastewater treatment plants, by integrating numerical multiphase models with advanced mechanical, biological and chemical processes, on WWTP units.

With regards to activated-sludge tanks, the incoming sludge will be first subjected to a primary sedimentation using grates, then will be subjected to other mechanical treatments like sand filtration and separation by settling. During the biological treatments, the organic matter and nutrients are removed, while the chemical treatment uses the precipitation to remove the phosphorous.

The work in this thesis is manly focused on the mentioned treatments applied to real wastewater treatment plants.

In the modern WWTP are widely used microbiological treatment, like activate sludge systems, where to remove the pollutants is exploited the bacterial biomass suspension. Organic matter is removed by adding oxygen to the suspended heterotrophic bacteria.

During the denitrifying process the nitrate produced with the sludge aeration, by autotrophic nitrifying bacteria, is turned into atmospheric nitrogen. In this phase known also as aerobic phase, take place the decay of the biomass that is balanced by the bacterial regrow.

So far, the majority of commercial WWTP models contains a detailed description of the biological and chemical processes occurring in wastewater treatment plant, whereas the hydrodynamic solution in each removal steps of the plant is modelled through rough assumptions of the mean flow properties.

Compared to the many existing commercial compartment models of WWTP, where each process tank typically is described through simplifying assumptions of the hydrodynamics, the application of a detailed hydrodynamic model, can in some way be regarded as a simpler way towards describing the process tank.

The study of a complete process tank model, that takes into account all sub processes occurring in each tank would be a very time demanding and complicated task for a single Ph.D. project.

Several of the processes involved in a process tank model have been extensively investigated by other researchers. The present work aims at combining these sub models into a whole process tank model. Towards the completion of a process tank model, several of the important sub processes will be investigated in a manner useful to the cause. The process tank model is as widely as possible constructed with

equally detailed process descriptions. There is no sense in modelling one sub process very detailed, if the result from such a detailed sub model disappears in a crude model for the remainder of the tank.

One important feature of a WWTP process tank model is the ability to predict the variation in concentrations of e.g. suspended solids, nutrients, biomass fractions or oxygen. A good description of mixing properties and thereby the concentration gradients is crucial for the modelling of these variations.

In order to model the mixing properties of the flow, the processes that contribute to both mixing and separation of substances needs to be accounted for in the model. Several of these processes are studied in detail in the present work:

- Anaerobic digester (Chapter 5);
- Disinfection tank (Chapter 6);
- Secondary settler (Chapter 7);
- Oxygenation tank (Chapter 8).

3.1 Results validation

One of the recent approaches to study the hydrodynamic mechanisms of WWTPs that turned to be even the more efficient is the use of numerical investigation to optimize plant design. In order to validate the mentioned approach is required to follow other tools. It can be used a design of an existing unit or use a theoretical model like the pilot-scale to validate the numerical model.

In a full-scale real unit, is represented the real behavior of the phenomena this imply the absence of approximation errors and consequently improve the accuracy of the data for the model validation. When not achievable, a pilot-scale can be used in order to locally represent the phenomena and then extend the results to the overall unit.

The first step to validate a numerical model is performed using the mass balance on which all the simulation study cases are based. A mass balance model of an ideal mixed reactor could be represented as:

$$Q_{out} = Q_{in} + \frac{dV}{dt} \tag{3.1}$$

Mass balance substances:

$$Q_{out}C_{out} = Q_{in}C_{in} + \frac{dV\bar{C}}{dt} \tag{3.2}$$

Where Q is the flow through the reactor $[m^3\ s^{-1}]$, V is the reactor volume $[m^3]$, C is the substance concentration $[kg\ m^{-3}]$ and $\bar{C}$ is the mean concentration $[kg\ m^{-3}]$:

$$\bar{C} = \frac{1}{V}\int_V Cdy \qquad\qquad (3.3)$$

In the equations (3.1) and (3.2), the last term on the right end side refers to the accumulation within the tank. The accumulation term can include the removal of substances by e.g. biological or chemical processes. In the mass balance model presented above the concentration strongly characterize the information that can be obtained from such a model. In these simulations is important to assume that the hydrodynamic conditions, to describe the flow of water and substances in the system, justify the use of a particular model.

The hydrodynamics of the mean flow, the turbulence and the settling, the aeration and the mixing processes are the characteristics used to describe the complex flow behavior in the units. It's important to underline that is impossible to describe the hydrodynamic field starting from the concentration outputs.

If a hierarchical structure was to be applied to the three above-listed processes, the hydrodynamic model would be located on the top. The explanation for this is to be found in the nature of the hydrodynamic multiphase model, where parameters like the fraction of air bubbles and the concentration of suspended solids can be directly extracted from the model. Thus, important parameters on which the results of the biological and chemical models are dependent of, is available as a result of the hydrodynamic model.

4. Governing Equation

4.1 Introduction

Computational fluid dynamics, CFD, is part of a growing number of development processes. In many situations, the liquid flow is not enough to represent the entire process, because it could be influenced by others parameters. For example, in a secondary settler the suspended solid concentration affects the flow parameters, or in an anaerobic digester the flow could be affected by the pressure which mix the sludge.

In a turbulent regime, vortexes may have a large variability, indeed, the turbulence is intrinsically chaotic: it is characterized by the presence of vortexes of different size. Larger vortexes transfer their kinetic energy to the smaller up to the point where a certain amount is permanently converted into heat. Turbulence can be therefore actively adopted as a system to dissipate energy.

Turbulence can be mathematically described by means of special dedicated models. The related computational burden can be expensive on the basis of the specific adopted paradigms. Among the others, in the Direct Numeric Simulation (DNS) turbulence model with reference to incompressible liquids is the most accurate way to simulate the fluid flows but the computational cost is very high. A dense discretization of space and time may require expected computation costs prohibitive to the actual state of power computing. The required accuracy may therefore involve the use of supercomputers or mainframes. In industrial applications effective turbulence models that speed up the computational time are often adopted with generally reasonable results. The most common used in this field is the k-ε model, in the following part it will be presented.

4.2 The Navier Stokes equations

At the core of most CFD software are the Navier Stokes (NS) equations. They comprehend the viscous term, respect to the Euler equations which stand for the inviscid flows. NS analytically describe the conservation laws for mass and momentum of Newtonian fluids as well as non-Newtonian ones, by introducing a modification in the viscous term. In a simplified way, the Navier Stokes equations for incompressible flows can be written as follows:

$$\rho \frac{\partial \boldsymbol{u}}{\partial t} + \rho(\boldsymbol{u} \cdot \nabla)\boldsymbol{u} = \nabla \cdot [-p\mathbf{I} + \mu(\nabla\boldsymbol{u} + (\nabla\boldsymbol{u})^T)] + \mathbf{F} - \rho\nabla \cdot \boldsymbol{u} \quad (4.1)$$

$$\rho\nabla \cdot \boldsymbol{u} = 0 \tag{4.2}$$

where $\boldsymbol{u}$ is the velocity vector, p is the pressure, ρ represents the density, t the time and finally μ is the turbulent viscosity of the fluid.

NS are a set of four coupled non-linear partial differential equations (PDEs) in which appear the three components for the local velocity $\boldsymbol{u}$ (3D space) and the pressure. The nonlinearity occurs mainly because of the momentum advection term $(\boldsymbol{u} \cdot \nabla)\boldsymbol{u}$, which is responsible for the chaotic behavior of turbulent flows. Once the flow has become turbulent, all quantities fluctuate in time and space. Numerical schemes in CFD models for solving the Navier-Stokes equations need to fully consider these characteristics (velocity – pressure coupling and nonlinearity).

4.3   The k-ε Turbulence Model

The k-ε model is the most used turbulence model, although it doesn't perform well in cases of large adverse pressure gradients. It is a two-equation model that means, it includes two extra transport equations to represent the turbulent properties of the flow. This two-equation represent the transport of turbulent kinetic energy k and the variable of turbulent dissipation ε.

The transport equation for k is:

$$\rho \frac{\partial k}{\partial t} + \rho\boldsymbol{u} \cdot \nabla k = \nabla \cdot \left[\left(\mu + \frac{\mu_T}{\sigma_k}\right)\nabla k\right] + \mathrm{P_k} - \rho\varepsilon \tag{4.3}$$

The k variable represents kinetic energy in the turbulent flux and the turbulent viscosity, μ_T is:

$$\mu_T = \rho C_\mu \frac{k^2}{\varepsilon} \tag{4.4}$$

C_μ is a model constant show in Tab. 4.1.

the production term P_k in the (4.3) is:

$$P_k = \mu_T\left(\nabla\boldsymbol{u}\colon(\nabla\boldsymbol{u} + (\nabla\boldsymbol{u})^T) - \frac{2}{3}(\nabla \cdot \boldsymbol{u})^2\right) - \frac{2}{3}\rho k\nabla \cdot \boldsymbol{u} \tag{4.5}$$

The transport equation for ε is:

$$\rho \frac{\partial \varepsilon}{\partial t} + \rho \boldsymbol{u} \cdot \nabla \varepsilon = \nabla \cdot \left[\left(\mu + \frac{\mu_T}{\sigma_\varepsilon} \right) \nabla \varepsilon \right] + C_{\varepsilon 1} \frac{\varepsilon}{k} P_k - C_{\varepsilon 2} \rho \frac{\varepsilon^2}{k} \qquad (4.6)$$

The variable ε is the rate of the viscous dissipation and the model constants $C_{\varepsilon 1}$, $C_{\varepsilon 2}$, σ_k and σ_ε are shown in the following Tab. 4.1.

The standard values of the constant in the (4.3), (4.4) and (4.6)**Errore. L'origine riferimento non è stata trovata.** are given as follows:

Tab. 4.1 – Model Constants

MODEL CONSTANTS	
Constant	**Value**
C_μ	0.09
C_{e1}	1.44
C_{e2}	1.92
s_k	1.0
s_e	1.3

The k-ε model uses the transport equation of kinetic energy (4.3) in conjunction with a transport equation for the rate of viscous dissipation (4.6) ε. The modelled ε equation is based entirely on empirical physical reasoning and dimensional arguments.

The above k-ε model equations are valid only sufficiently far from solid boundaries. There are three primary effects imparted by the wall on the structure of turbulence: turbulent eddies are distorted and constrained in size, being compressed in the wall-normal direction and elongated in the streamwise direction; production of turbulence increases due to the no-slip condition and intensification due to stretching of fluctuating vorticity; and turbulence energy is damped and dissipated into heat via viscous action.

Sometimes the solution of equation (4.4) and (4.5) can have a division by zero because the mixing length is used to calculate the turbulent viscosity. In order to avoid this issue, the implementation can include an upper limit on the mixing length, l_{mix}^{lim}:

$$l_{mix} = max \left(C_\mu \frac{k^{3/2}}{\varepsilon}, l_{mix}^{lim} \right) \qquad (4.7)$$

4.3.1   Model limitations

The k-ε turbulence model relies on several assumptions, the most important of which is that the Reynolds number is high enough. It is also important that the turbulence is in equilibrium in boundary layers, which means that production equals dissipation. These assumptions limit the accuracy of the model because they are not always true. It does not, for example, respond correctly to flows with adverse pressure gradients and can result in under-prediction of the spatial extent of recirculation zones (Wilcox, 1998). Furthermore, in simulations of rotating flows, the model often shows poor agreement with experimental data (Seegmiller et al., 1985). In most cases, the limited accuracy is a fair trade-off for the amount of computational resources saved compared to using more complicated turbulence models.

4.3.2   Wall Functions

Due to the highly empirical nature of the ε-equation the model equations become ill-conditioned as the wall is approached and need to be modified to account for the effects of the wall on the local structure of turbulence as well as to allow stable and robust implementation of the model in numerical computations (Pettersson et al., 2001). This means that the assumptions used to derive the k-ε model are not valid close to the walls. Even if it is possible to modify the k-ε model so that it describes the flow in wall regions, this is not always the best solution due to the very high-resolution requirements. Instead, analytical expressions are used to describe the flow near the walls, these expressions are known as wall functions. Since the structure of turbulence near the wall is dominated by the wall itself, it is assumed that the near-wall the flow depends on intrinsic variables.

A custom approach for wall functions is to assume an offset from the physical wall as shown in Fig. 4.1.

Fig. 4.1 - The computational domain is located a distance δ_w from the wall.

Expressed in viscous units, the wall lift-off is defined as:

$$\delta_W^+ = max\left(\frac{h}{2}\frac{\rho C_\mu^{1/4}}{\mu}, 11.06\right) \tag{4.8}$$

The first argument is derived from the law of the wall. The second argument is the distance from the wall, in viscous units, where the logarithmic layer meets the viscous sublayer. This lower limit ensures that the wall functions remain non-singular for all Reynolds numbers.

The wall lift-off, δ_W, is defined as:

$$\delta_W = \frac{\delta_W^+\mu}{\rho u_\tau} \tag{4.9}$$

where u_τ is the friction velocity and it is defined by

$$u_\tau = max\left(C_\mu^{1/4}\sqrt{k}, \frac{\|u\|}{u^+}\right) \tag{4.10}$$

$$u^+ = \frac{1}{\kappa_V}\ln(\delta_W^+) + B \tag{4.11}$$

where in turn, κ_V, is the von Kárman constant (default value 0.41) and B is a constant that by default is set to 5.2. The definition of δ_W is such that it becomes h/2 when $\delta_W^+ > 11.6$, but it can become larger when the lower limit for δ_W^+, 11.06, takes effect. In wall function, the boundary conditions for the velocity is a no-penetration condition, it means that $\boldsymbol{u} \cdot \boldsymbol{n} = \boldsymbol{0}$ and a shear stress condition

$$n \cdot \sigma - (n \cdot \sigma \cdot n)n = -\rho u_\tau \frac{u}{u^+} \tag{4.12}$$

where

$$\sigma = \mu\left(\nabla\boldsymbol{u} + (\nabla\boldsymbol{u})^T\right) \tag{4.13}$$

being the viscous stress tensor.

4.4   Mixture Model

4.4.1   Mixture Model Equations

The mixture model is an Eulerian-Lagrangian approach. It has been extensively used in the literature to study solid-liquid and gas-liquid mixing kinds of problems (Martin et al., 2020). With this approach, the forces are balanced and solved on each element of the disperse phase and the fluid flow is solved based on the use of either of the following turbulence methods: direct numerical simulations (DNS), Large Eddy Simulations (LES), Reynolds-averaged Navier–Stokes equations (RANS).
There are several mixture models where there is a fluid called "continuous" with a drag force acting on the dispersed phase. To calculate the hydrodynamic field of the dispersed fluid, which is influenced by the hydrodynamic field of the continuous fluid, among the most used, we find the dispersed models and particle tracking.
In mixture models, dispersed fluid it's immiscible with the continuous one and can be represented by solid, liquid or gaseous particles.
In the dispersed models the dispersed fluid is calculated as a concentration's distribution of finite particles per unit surface or volume, depending on the case being analysed. The particles density is treated as a second fluid and are computed using NS equations.
In the particle tracking is different because the dispersed phase is not considered as particle's distribution but as a single particle having its own physical properties. The particle properties are so small in size to be considered negligible, such that do not affect the hydrodynamic field of the continuous fluid. Otherwise the Particles motion is driven by the hydrodynamics field of the Continuous Phase. Since the calculation of particle motion is independent of the motion of other particles, to determine the motion of all the particles a high computational cost is required. These mentioned Mixture Models will be analysed more in detail in the following chapters.
Fully resolved turbulent Eulerian-Lagrangian applications are usually limited to small scales and limited number of particles, due to the high computational cost (Ayranci et al., 2013; Derksen, 2003). With the unresolved approach, the fluid flow is solved at scales coarser than the particle size, describing the particle-particle interactions coupling the two phases with explicit expressions of the interphase with drag forces like Shiller & Neumann (1933). Even though this approach allows to simulate denser suspensions with respect to the fully resolved approach, unresolved CFD models has seldom been used to assess partially suspended conditions (Blais, 2016).

In COMSOL Multiphysics, the Mixture Model interfaces consider the particle-fluid combination as a single flowing continuum with macroscopic properties such as density and viscosity. The two phases consist of one dispersed phase and one continuous phase. The mixture model is valid if the continuous phase is a liquid, and the dispersed phase consists of solid particles, liquid droplets, or gas bubbles. The mixture model relies on the assumptions that the density of each phase is approximately constant, both phases present equal pressure field and the particle relaxation time is short compared to the time-scales of the flow.

In order to calculate the macroscopic characteristics, the mixture model uses the density average of both phases:

$$\rho = \rho_d \phi_d + \rho_c \phi_c \qquad (4.14)$$

where ϕ_c and ϕ_d denote the volume fractions of the continuous phase and the dispersed phase respectively, their units in SI are: m^3/m^3; instead the ρ_c and ρ_d are the continuous phase and dispersed density respectively, their units in SI are: kg/m^3

The relationship between the continuous phase and the dispersed phase volume fraction is:

$$\phi_c = 1 - \phi_d \qquad (4.15)$$

The volume flux for each phase is

$$\boldsymbol{j}_d = \phi_d \boldsymbol{u}_d \qquad (4.16)$$

$$\boldsymbol{j}_c = \phi_c \boldsymbol{u}_c \qquad (4.17)$$

where $\boldsymbol{u}_c$ and $\boldsymbol{u}_d$ are the continuous phase and the dispersed phase velocity vectors, respectively.

As already previously said, the mixture model uses a unique equation of Navier-Stokes to simulate both phases, indeed, mixture velocity used here is the volume-averaged flux density, or volume-averaged mixture velocity (or simply velocity vector) $\boldsymbol{j}$, defined as:

$$\boldsymbol{j} = \boldsymbol{j}_d + j_c \qquad (4.18)$$

The continuity equation for the mixture is

$$\rho_t + \nabla \cdot (\rho \boldsymbol{u}) = 0 \qquad (4.19)$$

In the Mixture Model interfaces it is assumed that the densities of both phases, ρ_c and ρ_d, are constant, and therefore the following alternative form of the continuity equation for the mixture is used:

$$\nabla \cdot \boldsymbol{j} = m_{dc} \left(\frac{1}{\rho_c} - \frac{1}{\rho_d} \right) \tag{4.20}$$

The momentum equation for the mixture is

$$
\begin{aligned}
\rho \boldsymbol{j_t} + \rho (\boldsymbol{j} \cdot \nabla) \boldsymbol{j} + \rho_c \varepsilon (\boldsymbol{j}_{slip} \cdot \nabla) \boldsymbol{j} \\
= -\nabla p - \nabla \cdot \tau_{Gm} + \rho \boldsymbol{g} + \boldsymbol{F} - \nabla \\
\cdot \left[\rho_c (1 + \phi_c \varepsilon) \boldsymbol{u}_{slip} \boldsymbol{j}_{slip}{}^T \right] \\
- \rho_c \varepsilon \left[(\boldsymbol{j} \cdot \nabla) \boldsymbol{j}_{slip} + (\nabla \cdot (D_{md} \nabla \phi_d)) \boldsymbol{j} \right. \\
\left. + \boldsymbol{j}_{slip} m_{dc} \left(\frac{1}{\rho_c} - \frac{1}{\rho_d} \right) \right]
\end{aligned} \tag{4.21}
$$

where:
- $\boldsymbol{j}$ [m/s] is the velocity vector
- ρ [kg/m³] is the density
- p [Pa] is the pressure
- D_{md} [m²/s] is a turbulent dispersion coefficient
- m_{dc} [kg/(m³·s)] is the mass transfer rate from the dispersed to the continuous
- $\boldsymbol{g}$ [m/s²] is the gravity vector
- $\boldsymbol{F}$ [N/m³] is any additional volume force
- $\boldsymbol{j}_{slip}$ [m/s] is the slip flux defined as $\boldsymbol{j}_{slip} = \phi_c \phi_d \boldsymbol{u}_{slip}$
- $\boldsymbol{u}_{slip}$ [m/s] is the slip velocity vector between the two phases and it depends on the slip model used
- ε [kg/kg] is the reduced density difference and given by $\varepsilon = \frac{\rho_d - \rho_c}{\rho_c}$
- τ_{Gm} [kg/(m·s²)] is the sum of the viscous and turbulent stresses i.e.

$$\tau_{Gm} = (\mu + \mu_T)[\nabla \boldsymbol{j} + \nabla \boldsymbol{j}^T] - \frac{2}{3}(\mu + \mu_T)(\nabla \boldsymbol{j})\boldsymbol{I} - \frac{2}{3}\rho k \boldsymbol{I} \tag{4.22}$$

where μ is the mixture viscosity, μ_T the turbulent viscosity, and k is the turbulent kinetic energy.
In the multiphase flow the transport equation for the dispersed phase volume fraction, is:

$$\frac{\partial}{\partial t}(\phi_d\rho_d) + \nabla \cdot (\phi_d\rho_d\boldsymbol{u}_d) = \nabla \cdot (\rho_d D_{md}\nabla\phi_d) - m_{dc} \qquad (4.23)$$

This equation represents the variation in the time of the dispersed phase distribution, valid for solid and gas dispersed phases. The m_{dc} is the mass transfer rate from the dispersed to the continuous phase and D_{md} is the turbulent dispersion coefficient, accounting for extra diffusion due to turbulent eddies. Assuming constant density for the dispersed phase and using (4.20), (4.23) can be rewritten as:

$$\frac{\partial}{\partial t}(\phi_d) + \boldsymbol{j} \cdot \nabla\phi_d + \nabla \cdot (\boldsymbol{j}_{slip}) = \nabla \cdot (D_{md}\nabla\phi_d) - \frac{m_{dc}\rho}{\rho_d\rho_c} \qquad (4.24)$$

It is possible to account for mass transfer between the two phases by specifying an expression for the mass transfer rate from the dispersed phase to the continuous m_{dc}. The mass transfer rate typically depends on the interfacial area between the two phases. In order to determine the interfacial area, it is necessary to calculate the dispersed phase number density in addition to the phase volume fraction. The Mixture Model interface assumes that the particles can increase or decrease in size but not completely vanish, merge, or split. The conservation of the number density n then gives:

$$\frac{\partial n}{\partial t} + \boldsymbol{j} \cdot \nabla n + \nabla \cdot (n\phi_c\boldsymbol{u}_{slip}) = \nabla \cdot (D_{md}\nabla n) - nm_{dc}\left(\frac{1}{\rho_c} - \frac{1}{\rho_d}\right) \quad (4.25)$$

4.4.2   Dispersed Phase Boundary condition

Besides the need to set boundary conditions for the fluid flow, a multiphase simulation requires boundary conditions for the dispersed phase as well. The characteristics of the mentioned boundary conditions are similar to the one for single phase flow.

It's mandatory to specify the boundary conditions for the dispersed phase, either they can be on the domain's edges or on the boundary surfaces.

Most common boundary layers are: Wall, Inlet, and Outlet nodes. The DISPERSED PHASE CONCENTRATION is the default for the Inlet node.

$$\phi_d = \phi_{d0} \qquad (4.26)$$

The equation (4.27) specify the dispersed phase volume fraction value in the first time-step of the simulation. The dispersed phase number density can be specified directly:

$$n = n_0 \qquad (4.27)$$

where the subscript "0" refers to the starting values.

The "dispersed phase outlet" can be designed imposing a pressure or a velocity $\boldsymbol{u}_d$ as input. In both cases the output will give the missed property velocity and pressure respectively. Moreover, no condition is imposed on the volume fractions at the boundary.

The most used boundary is the "wall" node. This condition represents boundaries where the dispersed phase flux through the boundary is zero:

$$\boldsymbol{n} \cdot (\phi_d \boldsymbol{u}_d) = 0 \qquad (4.28)$$

A useful boundary condition is the SYMMETRY condition. This represent a symmetry line or surface for the dispersed phase, and sets the dispersed phase flux through the boundary to zero as depicted in (4.28).

4.4.3   Turbulence modelling

In dense flows the mixture viscosity usually becomes high. In such cases, the flow is laminar and no turbulence modelling is necessary. In diluted flows, with a low dispersed phase volume fraction, the turbulence may be particularly relevant.

In the used software, COMSOL Multiphysics, the Mixture Model for Turbulent Flow interfaces include the turbulence models described in § 4.3.

The turbulence must be accounted for in the calculation of the dispersed phase volume fraction. This is accomplished by introducing a turbulent dispersion coefficient D_{md} in (4.21) as:

$$D_{md} = \frac{\mu_T}{\rho \sigma_T} \qquad (4.29)$$

where σ_T is the turbulent particle Schmidt number (dimensionless) that characterize the fluid flows in which there are simultaneous momentum and mass diffusion convection processes.

The particle Schmidt number is usually suggested a value ranging from 0.35 to 0.7.

4.4.4   Slip velocity model – Shiller-Neumann

The Mixture Model use the Schiller-Naumann model which denote the relative velocity between the two phases $\boldsymbol{u}_{slip}$:

$$\frac{3}{4}\frac{C_d}{d_d}|\boldsymbol{u}_{slip}|\boldsymbol{u}_{slip} = -\frac{(\rho - \rho_d)}{\rho_d}\left(-\boldsymbol{j}_t - (\boldsymbol{j}\cdot\nabla)\boldsymbol{j} + \boldsymbol{g} + \frac{\boldsymbol{F}}{\rho}\right) \qquad (4.30)$$

where C_d (dimensionless) is the particle drag coefficient. Essentially, interpret the relation as a balance between viscous drag and buoyancy forces acting on the dispersed phase.

$$C_d = \begin{cases} \dfrac{24}{Re_p}\left(1 + 0.15Re_p^{0.687}\right) & Re_p < 1000 \\ 0.44 & Re_p > 1000 \end{cases} \qquad (4.31)$$

where Re_p is the particle Reynolds Number:

$$Re_p = \frac{d_d\rho_c|\boldsymbol{u}_{slip}|}{\mu} \qquad (4.32)$$

valid for droplets Reynolds numbers, Re_p, smaller than 1000. Note that this definition of the particle Reynolds number uses the viscosity of the mixture and not the viscosity of the continuous phase. As a matter of fact, the drag force magnitude acting on a droplet depends on the drop diameter. A widely accepted hypothesis is to consider the drag force acting on each droplet or particle as function of the local velocity.

Note that this definition of the particle Reynolds number uses the viscosity of the mixture and not the viscosity of the continuous phase, as would be customary for a single particle in a pure fluid with viscosity μ_c. This choice incorporates the hindrance effect of the other particles on the slip velocity.

Because the particle Reynolds number depends on the slip velocity, an implicit equation must be solved to obtain the slip velocity. Therefore, the Mixture Model interfaces add an additional equation for

$$|\boldsymbol{u}_{slip}|^2 \qquad (4.33)$$

when the Schiller-Naumann slip model is used. The Schiller-Naumann model is particularly well-suited for solid particles in a liquid.

4.5   Particle tracking

The Particle Tracing for Fluid Flow computes the motion of particles in a fluid. Particle motion can be driven by different forces like drag, gravitational, electric, magnetic, and acoustophoretic radiation forces.

In order to use the particle tracking approach, the system should either be a dilute or dispersed flow. This means that the particles should occupy a very small fraction of the volume of the surrounding fluid, generally less than 1%. When the volume fraction of the particles is not so small, the computational costs will be higher and in that case is preferable to use the Mixture Model seen in the § 4.4.

It is important to realize that with the particle tracing approach, particles do not displace the fluid they occupy. Furthermore, the finite radius of the particle is considered negligible when detecting and applying particle-wall interactions.

Motion of microscopic and macroscopic sized particles is typically dominated by the drag force acting on particles immersed in a fluid. There are two phases in the system: a discrete phase consisting of bubbles, particles, or droplets, and a continuous phase in which the particles are immersed.

Particle velocity is coupled to the continuous phase velocity calculated using a fluid flow model such as Laminar Flow or Turbulent Flow. As a way to determine the particle position in every time steps of the domain, to the particle's velocity are added external forces that contribute to define their trajectory, are considered the particles velocity and the external forces that contribute to define their trajectory.

In a sparse flow, the continuous phase affects the motion of the particles via the drag force, but the particles don't have enough inertia to significantly perturb the continuous phase. This is usually true when the particles in the discrete phase are very small or have relatively low number density. This is often referred to as unidirectional coupling or one–way coupling. When modelling such a system, it is usually most efficient to solve for the continuous phase first, then compute the trajectories of the discrete particles in a separate study.
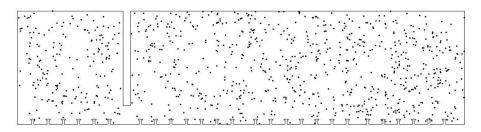

Fig. 4.2 – Example of particle distribution due to the velocity pattern

In a dilute flow the continuous phase affects the motion of the particles, and the particle motion in turn interact with the continuous phase. This is often referred to a bidirectional effect. The particles exert a volume force on the fluid at their location, equal in magnitude and opposite in direction to the total drag force exerted on the particles.

Compared to a sparse flow, the particles in a dilute flow typically have more inertia, due to the particles being bigger, denser, or more numerous. The computational demand is significantly higher when modelling dilute flows than sparse flows. Before setting up a bidirectional coupling, it is often beneficial to first set up the model with a unidirectional coupling and then determine whether the effect of the particles on the surrounding fluid is significant.

In a dispersed flow, the density of particles is greater than in the dilute flow, but their volume fraction is still lower than in a dense flow. The dispersed flow is the upper limit of the applicability of a Lagrangian particle tracking approach. In addition to the bidirectional fluid-particle interaction, particle-particle interactions may also need to be taken into account. This is sometimes referred to as four-way coupling.

The particle motion in a fluid is a combination of advective and diffusive transport. Advection is the bulk transport of particles by the mean fluid velocity via the drag force. Advection is typically deterministic, given a particle as a specified location in a laminar flow field, the motion of that particle at future times is completely predictable and reproducible. If a group of particles pass through the same point in the same stationary flow field, then all those particles will follow the same path.

There are two main mechanisms for diffusive transport in the particle tracing for fluid flow interface: molecular diffusion and turbulent dispersion.

Turbulence is the dominant mechanism for diffusive transport of macroscopic particles in a high Reynolds number flow.

Meanwhile for laminar flow, the drag force only contributes to the advective transport of the particles

$$F_D = \frac{1}{\tau_p} m_p (\boldsymbol{u} - \boldsymbol{v}) \tag{4.34}$$

but, if the flow is turbulent, then the fluid velocity u at the particle's position consists of a mean flow term $\overline{\boldsymbol{u}}$ and an instantaneous fluid velocity perturbation $\boldsymbol{u}'$,

$$\boldsymbol{u} = \overline{\boldsymbol{u}} + \boldsymbol{u}' \tag{4.35}$$

In a RANS model, eddies in a turbulent flow are not modelled explicitly; several different expressions for the perturbation term exist, the simplest being

$$\boldsymbol{u'} = \boldsymbol{\zeta}\sqrt{\frac{2k}{3}} \qquad\qquad (4.36)$$

where $\boldsymbol{\zeta}$ is a random unit vector and k is the turbulent kinetic energy.

Unlike molecular diffusion, turbulent diffusion has a finite resolution in time. If the time step taken by the solver is made extremely small, then eventually the turbulent perturbation term between successive iterations no longer consists of uncorrelated random vectors.

5. Anaerobic digester

5.1 Introduction

Anaerobic digestion is one of the most long-established processes for the stabilization of sewage sludge (Tchobanoglous et al., 2014). It is widely used to convert waste into valuable end products such as biogas (Lisowyj et al., 2020). A number of advantages can be ascribed to the use of anaerobic digestion. Anaerobic digestion can be employed to treat landfill leachate (Abuabdou et al., 2018; Abuabdou et al., 2020) a highly contaminated wastewater which when accidentally released into the environment poses a severe threat for aquifers, aquatic ecosystems and human health (Stoppiello et al., 2020).

Digesters in wastewater treatment plants to treat sewage sludge consist of insulated concrete or steel structures, usually cylindrical or egg-shaped, with a conical bottom from which the digested sludge is extracted. Recently, a renewed interest in anaerobic digesters (AD) has appeared. Factors such as sewage sludge disposal and the pursuit of climate protection objectives gave reason to re-think the classical, long established approaches concerning wastewater and sludge treatment for sewage treatment plants, even in the case of small to medium size (approximately 5,000 to 50,000 population equivalent) (Kariyama et al., 2018; Sadino-Riquelme et al., 2018; Wang et al., 2018). In Germany, for instance, MULEWF (Ministerium für Umwelt, Landwirtschaft, Ernährung, Weinbau und Forsten) and DWA (Deutsche Vereinigung für Wasserwirtschaft) reports proved that it is profitable to implement an anaerobic sludge digestion with biogas utilization in a co-generation unit for plant of small size against the common practice of aerobic simultaneous sludge stabilization. This new trend is giving a boost to the implementation of the anaerobic sludge digestion technology (Zare et al., 2019).

The anaerobic digestion process is sensitive to a large number of factors: temperature, retention time, nutrients concentration, pH and inhibitors concentration, mixing type and intensity (Dapelo D. , 2016). Temperature is a main factor affecting the process. Appels et al., (2008) recommended temperature variation within 0.6 °C per day. Solid (SRT) and hydraulic (HRT) retention times are important parameters as well, depending on geometry, flow rate, and recirculation system. The former indicates the average time that solids, and the bacteria living on them, spent inside the digester, while the latter refers to the liquid fraction.

Despite biomass retention being recognised among the most important parameters of anaerobic digestion providing SRT for the methanogens, poor biomass retention

in the conventional anaerobic digesters is often found (Lin et al., 2013; Shi et al., 1995). The pH is a key parameter related to the efficient running of a digester. Most fermentative bacteria can thrive in a wide range of pH, between 4.0 and 8.5, but their by-products depend on pH (Dapelo D. , 2016).

Effective anaerobic digestion is highly dependent on mixing system and frequency as well (Subramanian et al., 2015; Wang et al., 2019). Mixing promotes the establishment of a homogeneous environment for anaerobic digestion, by reducing temperature, concentration and other field gradients inside the reactor (Appels et al., 2008); Sindall et al., 2013). Meegoda et al. (2018) provided a comprehensive list of issues related to digester mixing.

Solid settling, short-circuiting, dead-zone, and scum formation arising from poor mixing are still major problems leading to less than optimal biogas production. Borole et al. (2006) proved that a pilot-scale digester with dairy manure yields continuous methane production with mixing, which soon deteriorates without agitation. Similarly, intermittent mixing is sometimes recommended (Lindmark et al., 2014; Leite et al., 2017). In fact, resting times can result in higher methane yield compared to continuous mixing while avoiding floating layer formation. The reason behind higher gas production is related to a balance reaching among microorganisms involved in the anaerobic conversion of biomass to methane. In addition, intermittent mixing is preferred to save energy compared with continuous mixing solutions (Singh et al., 2020). In addition, intermittent mixing results in lower power consumption and maintenance costs related to mixing solutions where two or more digesters are installed in parallel. In this case, it is possible to use one single biogas compressor, shared by the digesters, feeding the units alternately with biogas. On the contrary, continuous mixing requires several compressor units (usually one per digester) or a larger common compressor unit with a distribution and regulation system for biogas flow splitting.

There are three main mixing methods generally adopted in large-scale application of AD: mechanical mixing, gas mixing and pumped liquid recirculation through externally installed pumps or submerged jets (Qasim, 1999).

Mechanical stirring (Manea et al., 2012) can be done using: 1) low-speed with large impellers (one to three levels) without draft tube, installed on the digester roof; 2) high speed, vertical mixers with one small impeller with draft tube, installed on the digester roof; 3) high speed, inclined mixers with one small impeller installed through the digester wall. In all cases, the rotating impellers displace the sludge, mixing the digester contents. Low-speed turbines usually have one cover-mounted motor with two turbine impellers located at different sludge depths. Biogas production is affected by impeller design, eccentricity, bottom and inter impeller clearance, baffles and position of draft tube. Incorrect choice of impellers and

operating speed can lead to ineffective mixing. (Singh et al., 2019) reported that the geometry of the impeller has a significant effect on digester performance. The impeller should be chosen considering sludge rheology and turbulence to achieve an optimum design (Wu, 2010; Lindmark et al., 2014; Torotwa et al.,, 2018).

In gas mixing systems (Chandran et al., 2017; Serna-Maza et al., 2017), gas recirculation inside the digester acts as mixer. They can be unconfined or confined: the former are designed to collect biogas at the top of the digesters, compress and then discharge it through a series of bottom diffusers or radially placed top-mounted lances. In the latter systems, biogas is collected at the top of the anaerobic digesters, compressed, and discharged through confined tubes where an airlift effect is induced. The design of gas mixing systems is currently based on empirical correlations using the power input per unit volume $[W/m^3]$, the gas flowrate per unit volume of sludge $[m^3/(h\,m^3)]$, total solids (TS) [%], sludge rheology, and digester aspect ratio. Gas mixing systems have the advantage that they do not need moving parts installed inside the digester (Lindmark et al., 2014).

Pumping systems withdraw a portion of the biomass and reinject it tangentially through nozzles at the bottom of the tank (Sajjadi et al., 2016). This type of mixing, however, has been reported to be the least effective and has been rarely used alone for mixing (Tang, 2009). Pumped recirculation does not increase the mixing, despite it having a strong influence on flow pattern (Meister et al., 2018).

Vesvikar et al. (2005) indicated that areas in which the speed was less than 5% of the maximum speed were considered as dead or inactive zones. Formation of dead zones depends on the viscosity of slurry which increases with the increasing of the TS content, as later shown in the sludge rheology sub-section. To quantify velocity fields, (Wu, 2010) defined three velocity ranges:

- areas with low velocity (0 < v < 0.05 m/s),
- areas with medium velocity (0.05 < v < 1 m/s),
- areas with high velocity (v > 1 m/s).

Although computational fluid dynamics (CFD) is widely applied to investigate environmental flows (Blocken et al., 2012; Amicarelli et al., 2020) as it enables the numerical simulation of flow patterns as well as various output parameters in anaerobic digesters, e.g. vorticity, turbulence levels, etc., the number of CFD studies on anaerobic digestion is still limited.

The main challenge arises in the attempt of successfully simulating a time varying process, solving the Navier-Stokes equations adapted to account for the presence of a non-Newtonian fluid flow. Investigations of digester mixing using CFD have been performed by many researchers. (e.g. Wu et al., 2008; Terashima, et al., 2009; Martínez Mendoza et al., 2011; Wu, 2011; Wu, 2012; Wu, 2014; Dapelo et al., 2015;

López-Jiménez et al., 2015; Dapelo et al., 2018; Leonzio, 2018 and Meister et al., 2018). Wu & Chen, (2008) demonstrated that flow patterns for Newtonian and non-Newtonian fluids are completely different. Tab. 5.1 summarizes applied CFD numerical methods for discretizing governing equations, turbulence models and main outcomes for the above discussed reports.

Tab. 5.1 - Applied CFD methods, turbulence models and main results obtained in the surveyed literature.

Reference	CFD method	Turbulence model	Main results
Vesvikar & Al-Dahhn (2005)	Finite difference	k-ε for liquid phase, zero equation model for gas phase	Dead zones, flow pattern, gas distribution
Wu & Chen (2008)	Finite volume	k-ε for sludge treated as single equivalent phase	Dead zones, flow pattern
Terashima *et al.* (2009)	Finite element	No turbulence, homogeneous single-phase treated as laminar	Sludge concentration in full-scale anaerobic digester
Wu (2010)	multiple reference frame (MRF) for propeller	k-ε for sludge treated as single equivalent phase	Dead zones, Mixing energy level (Eq. 2)
Wu (2011)	multiple reference frame (MRF) for propeller	k–ε model, RNG k–ε, realizable k–ε (Shih et al. 1995), standard k–ω, SST k–ω, Reynolds stress model	Flow pattern, power and flow number (Paul *et al.* 2004)
Wu (2012)	multiple reference frame (MRF) for propeller	Large Eddy Simulation or sludge treated as single equivalent phase	Flow pattern, power and flow number (Paul . 2004)
Manea & Robescu (2012)	multiple reference frame (MRF) for propeller	No turbulence, homogeneous single-phase treated as laminar	Flow pattern, impeller geometry optimization
Wu (2014)	Eulerian multiphase flow model for gas mixing	SST k–ω model	Flow pattern, velocity gradient (Eq. 1), breakup number (Coufort. 2005)
Dapelo . (2015)	Euler-Lagrangian multiphase flow model for gas mixing	Reynolds stress model	Flow pattern, shear rate (Leonzio 2018)
Lopez-Jimenez et al. (2015)	Finite Volume method	k-ε for sludge treated as single equivalent phase	Dead zones, flow pattern, recirculation regions
Chandran et al. (2017)	Eulerian multiphase flow model for gas mixing	No turbulence	Velocity magnitude

Dapelo & Bridgeman (2018)	Euler-Lagrangian multiphase flow model for gas mixing	Reynolds stress model	Apparent viscosity (Eq. 4), Flow pattern, shear rate (Leonzio 2018)
Leonzio (2018)	Euler-Euler / Euler-Lagrangian multiphase flow model for gas mixing	k–ε model	Flow pattern, dead zones, shear rate
Torotwa & Ji (2018)	Euler-Euler multiphase flow model for gas mixing	k–ε model	Sludge concentration in laboratory-scale anaerobic digester. Flow pattern

Terashima, et al. (2009) evaluated the performance of the laminar flow agitation numerically, introducing the uniformity index parameter.

Martínez Mendoza et al. (2011) modelled the flow inside an anaerobic digester numerically, showing that the distribution of velocities and streamlines is vital for determining the occurrence of dead regions. (Manea et al., 2012) developed three-dimensional numerical simulations, obtaining the optimum geometry and nominal shaft speed for the digester under study. (Wu, 2011) applied six turbulence models (see Tab. 5.1) to predict mixing flow pattern in a full-size digester. Later on, (Wu, 2012) simulated the mixing agitation using the Large Eddy Simulation (LES) turbulence method, assuming the sludge as a pseudo-plastic. In this study, (Wu, 2012) used the sliding mesh method to characterize the impeller rotation.

Three sub-grid scale (SGS) models are investigated, namely the Smagorinsky-Lilly model, the wall-adapting local eddy-viscosity model and the kinetic energy transport (KET) model. Again, (Wu, 2014) simulated the gas mixture using a Eulerian multiphase flow model. The review paper of (Lindmark et al. 2014) summarized a number of CFD studies evaluating different mixing methods, their modelling approaches and validation methods. López-Jiménez et al., (2015) studied the anaerobic digester applying the Reynolds Averaged Navier-Stokes (RANS) equations closed with the standard k-ε turbulence model. A single-phase model was applied considering both Newtonian and non-Newtonian rheology for the sludge simulations, allowing the identification of dead zones as well as possible shortcuts.

(Leonzio, 2018) conducted research on the best mixing systems and geometric configuration for an anaerobic digester with CFD analysis. (Meister et al., 2018) performed a CFD analysis based on the finite volume method of the mixing of Newtonian and non-Newtonian sludge in anaerobic digesters to investigate the effects of operational variations on TS concentration. The study revealed that the operation with pumped recirculation and impeller rotating within a mechanical draft

tube yielded the highest level of mixing. Dapelo et al., (2018) developed a hybrid Euler-Lagrange (EL) CFD model to simulate an anaerobic digester mixed with gas under pressure. The movement of the sludge is driven by the transfer of the moment from the bubbles to the fluid. Recent comprehensive reviews on CFD applied to anaerobic digesters can be found in Sadino-Riquelme et al. (2018), Wang et al., (2018) and Singh et al. (2019).

Few reports dealing with the analysis of full-scale anaerobic digesters are available (Monteith et al., 1981; Kushkevych et al., 2020) because laboratory-scale digesters are typically adopted to evaluate a full-scale application of anaerobic digestion, see e.g. Wu & Chen (2008) and Bouallagui et al., (2010). However, scale effects could prevent a straightforward projection of operational data from laboratory-scale results to the full-scale designs.

In the following paragrapher will be shown a full-scale comparison of gas mixing and mechanical mixing of a pseudo-plastic sludge at same operational conditions. The simulation characteristics are: input/treated sludge (75 m^3/day), TS (6%), temperature T (35 °C) and daily energy consumption E (140.4 kWh). For this purpose, a CFD analysis was carried out, an approach where literature studies are still limited. The comparative analysis was carried out in terms of the distribution of velocity magnitude and pattern, turbulent kinetic energy and the formation of dead zones. Consumed energy E, derived from the real case consisting of a gas mixing anaerobic digester, was kept constant for two hypothetical cases consisting of two mechanical mixings, as next described.

5.2   Materials and methods

5.2.1   Case study description

The present fluid-dynamic investigation is referred to one of the two gas mixed anaerobic digesters of the Waste-water Treatment Plant (WWTP) connected to the municipality of Keszthely (Hungary). The WWTP is designed to serve 125,000 Population Equivalent (PE) as maximum during the touristic season (Fig. 5.1.a). Each digester is 11.30 m of inner diameter and 16 m high (14 m normal sludge filling level), for a sludge volume V=1,404 m^3 per digester.

a.

b.

Fig. 5.1 – a) WWTP in Keszthely (Hungary). Red circle indicates the position of the digesters. b) Inner side of one of the digesters with the gas recirculation lances.

The sludge quantity and composition are given in Tab. 5.2

Tab. 5.2 – Sludge quantity and composition (total for both digesters)

	Primary sludge	Biologic excess sludge
volumetric flow [m³/d]	83	68
dry solids (DS) concentration [kg/m3]	61	61
organic dry solids (ODS) [%]	71	61

In the actual configuration, eight vertical lances, 0.075 m of inner diameter and evenly spaced on a 4 m radius ring tube fed by a compressor, inject the biogas at a distance of 0.37 m from the bottom (Tab. 5.1.b). The gas mixing works

discontinuously, according to the sequence of 120 min divided into 6 phases of 20 min each, see Tab. 5.3. During each phase, a group of four adjacent lances is activated and fed with the full biogas flow delivered by the compressor.

Tab. 5.3 - Sequence of lances operations for the biogas mixing on the digesters, referred to as "A" and "B", respectively, of the Keszthely WWTP.

Phase nr.	1	2	3	4	5	6
Phase Duration [min]	20	20	20	20	20	20
Cumulative time [min]	20	40	60	80	100	120
Action	digester A, lances 1-4	pause	digester B, lances 1-4	digester A, lances 5-8	pause	digester B, lances 5-8

According to the operating conditions adopted for the digesters of the WWTP, the number of working hours in a day of the gas mixing system – considering one single digester – is therefore $n_h = 8$ overall. This modality was recently proved in Singh, et al., (2019) and Singh, et al., (2020) as the best to maximize biogas production in intermittent mixing. Daily energy consumed by the compressor is calculated by means of the following equation

$$E = \frac{Q_g \; dp \; p_s n_h}{1000} \; [\text{kWh}] \qquad\qquad (5.1)$$

where Q_g =282 Nm³/h is the total biogas flow rate at normal conditions delivered by the compressor, dp = 1.457 kPa is the compressor discharge pressure, p_s = 42.86 Wh/(Nm³kPa) is the compressor specific power consumption (Tab. 5.4).
Two long shafted paddle mixing impellers are considered as possible alternatives to the gas mixing system. The geometric specifications of the digester's shape and adopted mixers are summarized in Tab. 5.4.

Tab. 5.4 – Digester's geometry and adopted mixers

Digester inner diameter [m]	Digester total height [m]	Sludge filling level in digester [m]	Total Sludge Volume [m³]	Daily treated sludge Volume [m³/d]
11.30	16	14	1404	75
Gas Mixing	**Lances' outlet from bottom [m]**	**Discharge pressure [m_{H2O}]**	**Total gas volume flow rate [Nm³/h]**	**Specific power [Wh/(Nm³ kPa)]**
8 lances ϕ75 mm working alternated	0.37	1.457	282	42.86
Mixer 1	**Diameter [m]**	**Distance from the bottom [m]**	**Distance between impellers [m]**	

Propeller, 2 impellers, 2 blades per impeller	2.5	3.0	8.8
Mixer 2	**Diameter [m]**	**Distance to the bottom [m]**	**Distance between impellers (not equally spaced) [m]**
Propeller, 3 impellers, 2 blades per impeller	3.1	3.0	Upper spacing: 2.3 Lower spacing: 6.6

The rpm of the mixer blades is derived on the basis of the P – rpm relationship given in Tab. 5.10, Supplementary material.
The linear regression yields for Mixer 1:

$$P_1 = 0.2109 \, \text{rpm} - 0.4014 \quad R^2 = 0.9984 \qquad (5.2)$$

whereas Mixer 2 is well described by a linear function crossing the origin (0,0)

$$P_2 = 0.27 \, \text{rpm} \qquad (5.3)$$

Power consumption for mechanical mixing (working continuously h24) was derived by keeping constant E. Since the daily averaged power consumption for one digester is $\bar{P}$ = E/24 = 5.87 kW the number of revolutions therefore adopted are rpm_1 = 29.9 min^{-1} (from Equation (5.2)) and rpm_2 = 21.6 min^{-1} (from Equation (5.3)) for Mixer 1 and Mixer 2 respectively.

5.2.2   Sludge rheology

Sludge in anaerobic digesters, as wastewater, slurries from food processing plant and animal manure, exhibit a non-Newtonian behaviour (Sajjadi et al., 2016). In particular, slurry flows with TS ≥ 2.5% can be described as non-Newtonian pseudo-plastic fluids (Meister et al., 2018). From a general point of view, the stress tensor $\tau \, [Pa]$ is defined in terms of the shear rate tensor $\gamma' \, [s^{-1}]$ and the dynamic viscosity $\eta \, [Pa \, s]$

$$\tau_{ij} = \eta \gamma'_{ij} \qquad (5.4)$$

in which the shear rate components are given by

$$\gamma'_{ij} = \left(\frac{\partial u_i}{\partial x_j} + \frac{\partial u_j}{\partial x_i}\right) \qquad\qquad (5.5)$$

u_i is the scalar component of velocity field $\vec{v}$, along the x_i-coordinate axis.

In this study, the viscosity appearing in Equation (5.4) is modelled as function of the shear rate magnitude $|\gamma'|$ using a power-law relationship (Rendina, Viccione, & Cascini, 2019):

$$\eta = K|\gamma'|^{n-1} \qquad\qquad (5.6)$$

where K is the consistency coefficient and n is the power law index. Equation holds for the interval $\zeta = (|\gamma'|_{min}; +|\gamma'|_{max})$ depending on the content of TS (Wu & Chen 2008, Bridgeman 2012), see Tab. 5.5. Beyond ζ limits, viscosity takes a constant minimum η_{min} and maximum η_{max} values to prevent singularities when computing runs take place. Rheology parameters strongly depend on TS (Wu et al., 2008) and temperature T as depicted in Tab. 5.5 (Achkari-Begdouri et al., 1992).

Tab. 5.5 – Rheological properties of sludge at T=35°C

TS [%]	K [Pa s^n]	n [-]	η_{min} [Pa s]	η_{max} [Pa s]	ρ [kg / m^3]	ζ [s^{-1}]
2.5	0.042	0.710	0.006	0.008	1000.36	226-702
5.4	0.192	0.562	0.01	0.03	1000.78	50-702
7.5	0.525	0.533	0.03	0.17	1001.00	11-399
9.1	1.052	0.467	0.07	0.29	1001.31	11-156
12.1	5.885	0.367	0.25	2.93	1001.73	3-149

From Fig. 5.5 the following regressions, either linear or exponential, are derived:

$$K = 0.0117\, e^{0.5078\, TS} \qquad R^2 = 0.9983 \qquad (5.7)$$

$$n = -0.034\, TS + 0.7793 \qquad R^2 = 0.9777 \qquad (5.8)$$

$$\rho = 0.1425\, TS + 999.99 \qquad R^2 = 0.9956 \qquad (5.9)$$

Parameters' values were derived from regressions, Equations (5.7)-(5.9), assuming the sludge isothermal and incompressible, see Tab. 5.6.

Tab. 5.6 – Derived parameters' values for the sludge at T= 35°C with TS=6%.

TS [%]	K [Pa s^n]	n [-]	ρ [kg / m^3]
6	0.246	0.575	1000.85

5.2.3   Numerical setup

The Level Set Two-Phase Flow method (Olsson et al., 2005; Bovolin et al., 2017) is adopted to model fluid – gas interaction in the case of gas mixing. The Level Set method allows to simulate two immiscible fluids separated by moving interfaces making use of a level set function, that is a smooth continuous function $\varphi[\vec{x}(t)] \in [0,1]$ which value defines the phase locally:

$$\varphi \begin{cases} > 0.5 & Fluid \\ = 0.5 & Interface \\ < 0.5 & Air \end{cases} \tag{5.10}$$

The evolution of φ is described by the following transport equation:

$$\vec{v}\,\vec{\nabla}\varphi = \gamma\vec{\nabla}\cdot\left(\varepsilon\vec{\nabla}\varphi - \varphi(1-\varphi)\vec{\mathbf{n}}\right) \tag{5.11}$$

where ε and γ are the stabilization and reinitialization terms respectively, $\vec{\mathbf{n}} = \frac{\vec{\nabla}\varphi}{|\vec{\nabla}\varphi|}$ is the unit normal vector. Sludge motion is modelled as incompressible, spatially integrating over a finite element grid the unsteady Reynolds-Averaged Navier–Stokes (RANS) equations, modified for Non-Newtonian rheology:

$$\nabla \cdot \vec{v} = \vec{\mathbf{0}} \tag{5.12}$$

$$\rho\left(\frac{\partial}{\partial t} + \vec{v}\vec{\nabla}\right)\vec{v} = -\vec{\nabla}p + \vec{\nabla}\tau + \rho\vec{g} + \sigma\kappa\delta\vec{\mathbf{n}} \tag{5.13}$$

where the τ i and j components are given by Equation (5.4), $\vec{\nabla}$ is the symbolic operator of components $\left(\frac{\partial}{\partial x}, \frac{\partial}{\partial y}, \frac{\partial}{\partial z}\right)$, $\vec{v}$ is the velocity field, $\vec{g}$ is the gravity acceleration, p is the pressure, "·" is the symbol of the scalar product,

$$\rho = \rho_a + (\rho_f - \rho_a)\varphi \tag{5.14}$$

$$\eta = \eta_f + (\eta_f - \eta_a)\varphi \tag{5.15}$$

are the local density and the dynamic viscosity obtained by linearly averaging between corresponding values for the fluid "f" and air "a". Last term on the right hand side of equation (5.13) represents the surface specific tension force which arises over interfaces: $\sigma = 0.0705\ N/m$ is the tension coefficient, here assumed as for water-air, δ is the Dirac delta function and $\kappa = \vec{\nabla}\cdot\vec{\mathbf{n}}$ is the local interface curvature

field. Turbulence is modelled using the standard two-equation k-ε model (Launder & Spalding, 1974), based on the transport equations for kinetic turbulent energy (k) and the dissipation rate (ε) (see § 4.3) has been successfully used by many researchers for related mixing problems in anaerobic digester (López-Jiménez, et al., 2015; Meroney et al., 2009).

Gas inlet is set at the lower end of four adjacent lances, each lance issuing a gas flow rate of 10.2 L/s. Gas outlet is set at the upper free surface of the sludge. Simulation domain corresponds to the inner space of digester with the presence of the eight lances, see Fig. 5.2.a.
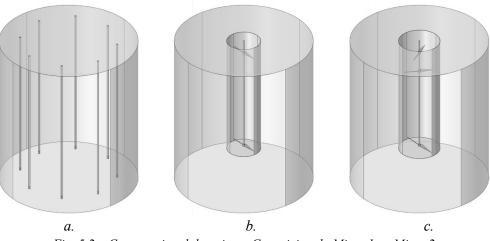

a.   *b.*   *c.*

Fig. 5.2 – Computational domain. a. Gas mixing. b. Mixer 1. c. Mixer 2

In the case of mechanical mixing (Fig. 5.2.b and Fig. 5.2.c), the rotating domain is modelled using a homogeneous single-phase turbulent non-Newtonian flow. The steady Navier-Stokes equations formulated in the rotating coordinate system:

$$\nabla \cdot \vec{v} = \vec{0} \tag{5.16}$$

$$\rho \vec{\mathbf{w}} \nabla \vec{\mathbf{w}} + 2\rho \vec{\mathbf{\Omega}} \times \vec{\mathbf{w}} = \vec{\nabla} p + \vec{\nabla} \cdot \boldsymbol{\tau} + \rho \left[\vec{\mathbf{g}} - \frac{\partial \vec{\mathbf{\Omega}}}{\partial t} \times \vec{\mathbf{r}} + \vec{\mathbf{\Omega}} \times \left(\vec{\mathbf{\Omega}} \times \vec{\mathbf{r}} \right) \right] \tag{5.17}$$

are solved with reference to the velocity vector $\vec{\mathbf{w}}$, referred to the rotating coordinate system. In the above Equations (5.16)-(4.36) $\vec{\mathbf{r}}$ is the position vector while $\vec{\mathbf{\Omega}}$ is the angular velocity vector. In the global coordinate system, the velocity vector $\vec{v}$ is related to the moving component $\vec{\mathbf{w}}$ by mean of:

$$\vec{v} = \vec{w} + \frac{\partial \vec{r}}{\partial t} \qquad\qquad (5.18)$$

5.2.4 Mesh generation and convergence study

In the case of gas mixing, the lances are treated as void spaces. The mesh is finer where gas inlet is set, since the inlet gas flow velocity is the highest in this region. In the case of mechanical mixing, two regions with different mesh quality are introduced. The mesh of the rotating domain is finer than the mesh of the rest of the domain since the flow velocity is higher in this region.

The spatial decomposition is made by using unstructured meshes of tetrahedral elements. Finer boundary layer mesh elements are set at the walls to comply with the constraints imposed by the adopted k-ε turbulence model. Sharp corners are avoided because they may introduce singularities in the solution.

Regarding the mesh convergence three levels of spatial discretization are tested, respectively indicated as mesh 1, 2 and 3 in Tab. 5.7 (gas mixing) and Tab. 5.8 (Mixer 1). The successive refined meshes yielded convergent solutions starting from mesh 2 for all cases, thus making the fluid structure interaction (FSI) computations reliable. Results next presented are obtained with such level of discretization.

Tab. 5.7 – Mesh properties in the case of Gas mixing

Mesh parameters	Mesh 1	Mesh 2	Mesh 3
Max cell size [m]	1.980	1.650	1.254
Min cell size [m]	0.099	0.099	0.0099
Number of cells	36 323	62 566	123 931

Tab. 5.8 – Mesh properties in the case of Mixer 1.

Mesh parameters	Mesh 1		Mesh 2		Mesh 3	
	Rotating Domain	Outer Domain	Rotating Domain	Outer Domain	Rotating Domain	Outer Domain
Max cell size [m]	0.0053	0.013	0.004	0.01	0.003	0.007
Min cell size [m]	0.01	0.006	0.001	0.005	0.001	0.004
Number of cells	26 696	204 432	41 094	334 752	66 766	672 912

5.3   Results and discussion

The evaluation of the mixing is done by computing the velocity magnitude and pattern, the turbulent kinetic energy and the formation of dead zones. Results are presented when nearly steady state conditions are reached as in (Viccione et al., 2012) in the case of gas mixing. Dead zones refer to the regions of the digester where the velocity is smaller than 0.05 m/s according to (Wu, 2010). Computed quantities are all referred to the inner volume Ω of the digester. The analysis of the velocity pattern shows that a convective movement of the sludge is created inside the digester; see Fig. 5.3. In the central section of the digester a large downward flow is created in the central part with vortexes located near the bottom of the digester. In the case of gas mixing (Fig. 5.3.a), higher velocity magnitudes are attained of the order of 1 m/s near the walls. This is basically due to the thrust exerted by air bubbles on the sludge when moving upwards to the free surface. In the case of mechanical mixing (Fig. 5.3 .b and Fig. 5.3 .c), the velocity magnitudes were generally dramatically lower, with peaks of 1.33 m/s nearby the paddle blades for Mixer 1 (see Fig. 5.4).
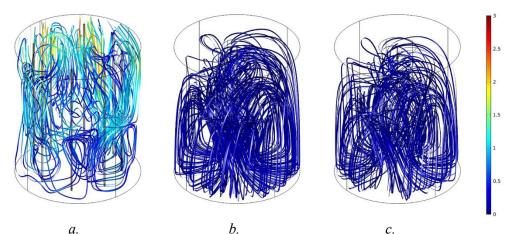

a.   *b.*   *c.*

Fig. 5.3 – 3D Trajectory extraction. Colour is related to the velocity magnitude [m/s]. a. Gas mixing. b. Mixer 1. c. Mixer 2.

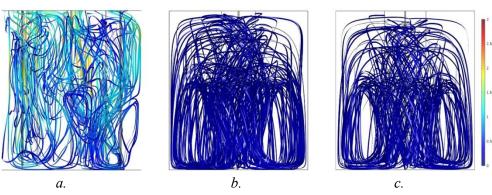*a.*   *b.*   *c.*

Fig. 5.4 – 2D Trajectory extraction. Colour is related to the velocity magnitude [m/s]. a)
Gas mixing. b) Mixer 1. c) Mixer 2.

The results concerning the turbulent kinetic energy $[m^2/s^2]$ reveal a level of agitation at the upper part of the digester with a maximum value of 0.24 m^2/s^2 in the case of gas mixing (Fig. 5.5.a). This is an expected result as the gas bubbles finally break at the free surface, generating turbulence nearby. From an operational point of view, this aspect is very useful because it helps the digester function against the formation of crusts. In the case of mechanical mixing, turbulence levels are negligible as can be seen in Fig. 5.5.b and Fig. 5.5.c.
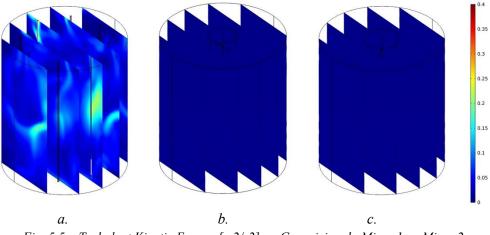

a.   *b.*   *c.*

Fig. 5.5 – Turbulent Kinetic Energy [m2/s2]. a. Gas mixing. b. Mixer 1. c. Mixer 2.

As concerning the formation of dead zones, half of the digester inner volume Ω participates actively in the mixing process. In the case of mechanical mixing (Fig. 5.6.b and Fig. 5.6.c) most of the stagnant regions are located near the vertical wall and at the free surface, whereas the inner regions near the paddle blades feature high levels of velocity.
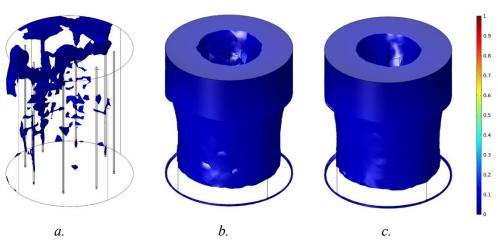
a.   *b.*   *c.*

Fig. 5.6 – Dead zones, defined on the basis of the condition v < 0.05m/s. Colour contour is set with the upper value (unity) related to the threshold velocity. a. Gas mixing. b. Mixer 1. c. Mixer 2.

In the case of gas mixing, dead zones are present far away from the gas inlet areas as depicted in Fig. 5.6.a, attaining the mean value of about 4.8% (see Tab. 5.9). Geometry optimization concerning the digester shape, length, distance to the bottom and diameter of lances would certainly allow a further decrease (Singh et al., 2019). In the following Tab. 5.9, a summary of the obtained numerical results is presented. The 'intermediate velocity zones' refers to the volume (in percentage in respect of the inner volume) where velocity ranges in the interval $0.05 < v < 1$ m/s, whereas the 'high velocity zones' refers to velocities higher than 1 m/s.

Tab. 5.9 – Main numerical results. Percentages between brackets refers to the inner volume Ω

Parameter	Gas mixing		Mixer 1	Mixer 2
	Mean value	Standard deviation		
Max velocity [m/s]	3.03	0.20	1.33	1.00
Spatially averaged velocity [m/s]	0.31	0.09	0.07	0.07
Spatially averaged turbulent kinetic energy [m^2/s^2]	0.23	0.10	0.001	0.001
Dead zones [m^3]	63.64 (**4.8%**)	42.08 (3.2%)	665.83 (50.6%)	674.91 (51.3%)
Intermediate velocity zones [m^3]	1237.64 (94.1%)	26.89 (2.0%)	649.12 (49.4%)	639.87 (48.7%)%

High velocity zones [m³]	13.68 (1.0%)	19.74 (1.5%)	0.00 (0.0%)	0.00 (0.0%)

The best solution, considering the same daily energy consumption E, is given by the gas mixing solution. In fact, in Tab. 5.9 it is shown that dead regions are about a tenth of mechanical mixing (4.8% vs 50.6% for Mixer 1 and 51.3% for Mixer 2) while spatially averaged velocity is about four times greater (0.31 m/s vs 0.07 m/s for Mixer 1 and Mixer 2). This is basically due to the corresponding low number of revolutions for the adopted Mixers ($rpm_1 = 29.9\ min^{-1}$ and $rpm_2 = 21.6\ min^{-1}$, respectively). In (López-Jiménez et al., 2015) the simulation of flow patterns was carried out using a propeller rotating from 400 to 750 rpm, which is one order of magnitude greater. Dead zones, however defined on the less restrictive criterion $v < 0.05\ m/s$ were 0.21% and 4.2% for non-Newtonian sludge with TS = 2.5% and 5.4% respectively. (Manea et al., 2012) recommended axial mixers having four to six blades, with a tilt angle between 15° and 45° and shaft speeds between 100 and 800 rpm. In addition, six new simulations (three per mixer) were carried out with the parameters listed in Tab. 5.6, to compare the effect of increased mixing speeds of 50, 100 and 200 rpm on the percentage of dead zones (DVP), without caring of the mixer rpm operational range (see specifications in Tab. 5.10).

Tab. 5.10 – P–rpm relationship for the adopted mechanical mixer

Mixer 1		Mixer 2	
rpm [min⁻¹]	**P [kW]**	**rpm [min⁻¹]**	**P [kW]**
2.5	0.36	12.5	3.40
5.6	0.68	50	13.60
14.8	2.53		
50	10.20		

Once again, dead volumes were assessed on the basis of the condition $v < 0.05\ m/s$. Results are summarized in Tab. 5.11.

Tab. 5.11 – Impact of mixing speed (rpm) on dead volume percentages (DVP) and consumed energy (E) for Mixer 1 and Mixer 2.

Mixer 1			Mixer 2		
rpm [min⁻¹]	**DVP [%]**	**E [kWh]**	**rpm [min⁻¹]**	**DVP [%]**	**E [kWh]**
29.9	50.6	140	21.6	51.3	140
50	21.6	243	50	2.9	324
100	0.4	496	100	0.1	648
150	0.1	750	200	0.0	972

Daily energy consumptions E are derived from Equations (5.1) and (5.3), for Mixers 1 and 2, respectively, under the same condition of mixing operating 24 h per day. As can be noted, the increase of rpm corresponds to a fast decrease of DVP but at the expense of higher E levels. Above rpm = 100, stagnant regions occupy less than 1% of the digester's volume, at the cost of tripled energy values or more, compared with the reference value E = 140.4 kWh. Geometry optimization of the mechanical mixing systems can lead to a drastic reduction of dead zones (Singh et al., 2019) as well. This implies a sensitivity analysis based on the geometry of the mixer (number of impellers, number of blades per impeller, the blade's profile) which is out of the scope of this study.

In terms of turbulent agitation, mechanical mixing does not exhibit significant levels, proving that this technology is appropriate only for convective movement.

5.4   Conclusions

Anaerobic digestion is largely applied for the stabilization of sewage sludge and landfill leachate. The production of biogas is beneficial for the environment, helping the reduction of greenhouse emissions. The efficiency of digestion process is affected by several operating parameters including the rate of mixing, which was commonly studied in the past at a laboratory scale.

In this study, a three-dimensional CFD steady/unsteady model was developed and applied to quantify mixing in a full-scale anaerobic digester. Non-Newtonian properties of the sludge, consisting of a pseudo-plastic fluid, were taken into account in the closure of governing equations. Stirred and gas mixing solutions were compared in terms of flow patterns, turbulent kinetic energy and dead zones, keeping fixed the daily energy consumption. In the case of gas mixing, the real configuration of the lances and their operating conditions were adopted. For the mechanical mixing, two central draft tube mixers with two (Mixer 1) and three (Mixer 2) impellers, respectively, were comparatively studied. The number of rounds per minute were derived from the given P–rpm curves, under continuous mixing. Gas mixing was found to be preferable to mechanical mixing in terms of mixing performances, namely:

- maximum velocity was about three times larger than that associated with mechanical mixing systems;
- dead zones percentage was one order of magnitude lower (about 5% against 50%);

- turbulent kinetic energy was two orders of magnitude larger ($0.24\ m^2/s^2$ against $0.001\ m^2/s^2$). Maximum values were reached over the upper part of the digester, with a positive effect against the formation of crusts.

Increasing impeller speed helps reduce stagnant regions but at the cost of higher electric energy consumption.

6. Disinfection tank

6.1 Introduction

A Computational Fluid Dynamic (CFD) study was carried out to characterize the distribution patterns of Peracetic Acid (PAA, CH_3CO_3H) in a full-scale disinfection tank with the aim of optimizing the reactor configuration to improve disinfection efficiency. The case of study refers to the wastewater treatment plant (WWTP) located in Nocera Superiore, Campania Region, Italy (Fig. 6.1), receiving wastewater collected from urban households, agro-industries, zootechnical activities, hospitals and other facilities. The WWTP had an average capacity of 300,000 PE., and a flow rate ranging between 30,000 $[m^3/d]$ (winter) up to 60,000 $[m^3/d]$ (summer) due to seasonal activities (e.g. cannery industries). The treatment process includes:

- Mechanical pre-treatment (screening and pumping stations, grit and oil removal);
- Rainwater section (primary sedimentation and aerated storage);
- Secondary treatment (nitrification-denitrification and final settling);
- Tertiary treatment (gravity filtration on sand),
- disinfection with peracetic acid.

Incoming wastewater characteristics strongly depend by the current season because the industrial sites in the area increase their productivity seasonally, generating different characteristics of the inlet, both in terms of flow rate and dissolved substances. For this reason, the efficiency of the disinfection process is a matter of particular interest for the context, representing the last step of the wastewater treatment plant before the treated effluent is released into the environment.

Fig. 6.1- The Nocera Superiore (Italy) wastewater treatment plant (WWTP). Red rectangle indicates the position of the contact tank.

PAA as well as other chemical disinfectants such as performic acid (PFA, CH_2O_3) undergoes to an instantaneous consumption, according to a kinetic of the first-order. The decay of PAA inside the tank follows the equation

$$\frac{\partial c(t)}{\partial t} = -kc(t) \qquad (1)$$

meaning that PAA concentration c decrease over the time. The k constant k=0.006 s-1 was measured during an experimental campaign.

The full-scale contact tank geometry, 28 m x 29.5 m x 3.5 m, was implemented in Comsol Multiphysics, see Fig. 6.2.a. Mixing is performed by a propeller (Figure 2.b) 1 m of diameter, a frequency equal to 180 min-1, that results a rotational speed (rpm) of 3 revolutions per second. The shaft is rotated of 70° respect to the vertical axis (main body direction), as shown in in Figure 2.a,). PAA is dosed at the free surface nearby the propeller as well as in the upstream heading tank of smaller size. The PAA measured in the inlet region of the contact tank is $c_0 = 0.8 \, mg/l$.

Outlet region

Impeller region
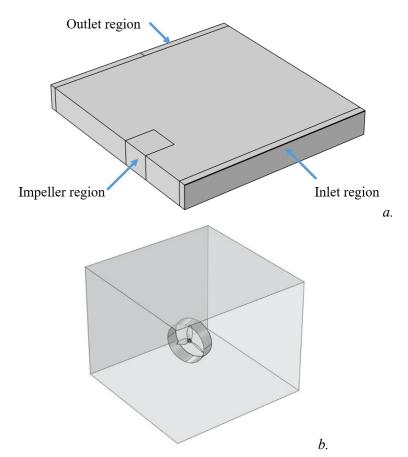
Inlet region

a.

b.

Fig. 6.2– a. Contact tank model's geometry. b. A particular of the propeller's blades.

The inlet flow rate Q = 1356 m^3/h corresponding to the annual average discharge at the contact tank was used for the modelling. Steady Reynolds Averaged Navier-Stokes (RANS) equations coupled with the standard k-ε turbulence model are numerically solved with the Finite Element Method (FEM) formulation. Spatial discretization is performed by dividing the simulation space (grey volume in Fig. 6.2.a) in 137,478 rectangular parallelepiped elements.

a.

b.

Fig. 6.3 – a. Steady state velocity contour, mainly induced by the propeller blades' motion and secondarily by the inlet and outlet regions. b. concentration [$\mathbf{mol/m^3}$] at the inlet (green line) and at the outlet (blue line)
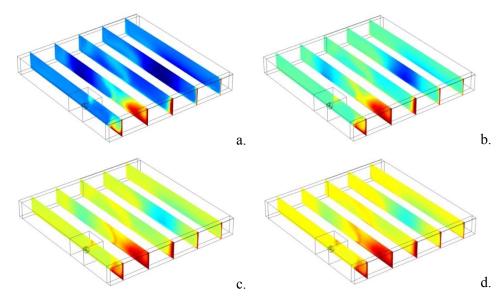

a.

b.

c.

d.

Fig. 6.4 – Transport of the diluted specie PAA at a. 500 s, b. 5000 s, c. 10000 s, d. 20000 s.

The numerical simulation consisted in two steps. The first one was aimed to solve the steady state hydrodynamics, e.g. no local variations of hydrodynamic quantities were taken into account (see Figure 3.a). Then the transport of the diluted PAA compound was run, taking as a reference the CFD patterns, previously obtained (Figure 4).

Transport phenomena approach the steady state asymptotically. As shown in Figures 3 and 4, the order of magnitude for the time needed to reach a steady distribution of PAA inside the tank is of several hours ($t_{asymp} = 20000/3600 \approx 6$ h). This is evident in Fig. 6.3.b where the PAA concentration at the outlet tend to the asymptotic value after a transitory period is resolved.

6.2   Conclusion

A full-scale disinfection tank was considered in this study with the aim to reproduce disinfection fate and transport via CFD.

Simulations were run in unsteady conditions. Once steady state was attained, the velocity field was extracted, showing that the area between the impeller and the inlet has very low speeds, which means that peracetic acid concentrations tend to accumulate in the "slow velocity" area. Indeed, a high concentration value was detected, as reported by on-site measurement campaigns.

To solve the problem of the high concentrations in the "slow velocity" area, internal septa could be set within the tank in order to force the water flow to follow an established path. This may promote the reaction between acid and water as a result of the greater contact time. In addition, there is a considerable energy saving as the impeller would no longer be necessary.

7. Secondary settler

7.1   Introduction

Industrial plants are generally required to release process water with concentrations of pollutants and Total Suspended Solids (TSS) below set limits. For this purpose, specific water treatment plants are used. The process of water treatment consists of various compartments capable of reducing the concentration of TSS.

In this chapter it is intended to analyse the secondary settler of a sugar factory located in Strzelin, Poland, characterized by a constant inlet concentration due to the use of the anaerobic digester located upstream of the settler. In addition, a recirculation flow rate of 180 m³/h is taken from the bottom of the settler to be reintroduced into the anaerobic digester in order to maintain a high concentration of sludge in the upstream unit.

The secondary settler is one of the units of the waste water treatment plant widely studied for complex phenomena that take place inside the tank, as supported by Samstag et al., (2016) and Stamou, (2008)

Generally, the sludge flocs are heavier than the water phase, they will settle out, and a distinct phase discrimination between the water phase and the sludge flocs will develop, if no external mixing is applied to the system.

The aim of this study is to optimize through a Computational Fluid Dynamic approach the geometric shape of the deflector placed in the centre of the tank. The expected result is a lower outlet concentration, in the clarified outlet, with respect to the designed one. The used tool to obtain the optimization is the Froude densiometric number, explained in the following chapter § 7.5.

7.2   Study case

The Strzelin settler (Figure 1.a) has a circular shape, with a radius of 14 m with a column in the centre, having a radius of 30 cm, which support the overhead crane. In the central area, near to the column, where is pumped a sludge flow rate of 305 m^3/h with a concentration of TSS of 50 g/l.

The corresponding computational domain has been implemented in COMSOL Multiphysics. The software allows to simulate the processes that take place inside the settler through the mixture model, capable of reproducing the space-time trend of the dispersed phase.

The model is made up of a single solid dispersed phase, consisting of particles with an average diameter of 0.15 mm and a density of 1300 kg/m^3. The incoming flow is contained by a circular deflector with a diameter of 1,765 m and a depth of 4 m; at a distance of 25 cm from the bottom of the deflector, a "cap" made of a wall tilted by 25° with respect to the horizontal, is placed.

For this type of geometry, central symmetry has been adopted in order to use an axial-symmetric 2D model, neglecting hydrodynamic components in the transverse dimension. Using this assumption allows to greatly speed up the calculation time, reducing the number of mesh elements, without affect the accuracy of the result compared to 3D simulations (Armbruster et al., 2001). To optimize the calculation time, the mesh elements are denser near the inlet, the two outlets and at the bottom where the solid phase is expected to settle.

Boundary conditions are set on the contours of the model as representative of the surfaces that are obtained by revolution around the central symmetry axis. In Figure 1.b, the two-dimensional model consists:

- Constant inlet flow at the top left;
- Clarified outlet condition with no pressure at the top right end side,
- Recirculation outlet with constant velocity in the lower left part,
- Wall condition with sliding to simulate the constant water surface of the settler
- Wall condition for each of the other segments;

the overall the domain is subjected to gravity force that allows the sedimentation of the solid part inside the settler.
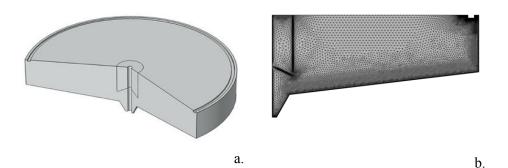

a.   b.

Fig. 7.1 – a. Isometric view of settler geometry obtained by 2D section revolution around the central symmetry axis; a. Mesh

7.3   Model equations

COMSOL Multiphysics adopts the mixture model for the approximate calculation of the Navier–Stokes equations on a system consisting of a continuous phase and a dispersed one. The effects of turbulence are included with a k-ε model, with a constant turbulent viscosity (Krebs, 1991). The pressure distribution is mediated by the mixture continuity equation and the dispersed phase velocity is described by the slip model as seen in §4.4.4.

In this way it is possible to know the hydrodynamic field of the mixture which is composed by two phases. The simulation involves a continuous phase, made of water, and a dispersed phase represented by suspended solids, that are immiscible with the continuous phase.

7.4   Sludge rheology

According to Barnes (2000), Rheology is: the study of the flow and deformation of materials. In this section, equations describing the rheology of the suspension in a process tanks will be outlined.

The continuous phase carrying the dispersed phase in suspension in the process tank is essentially the Newtonian Fluid, Water. All Newtonian fluids obey Newton's law of viscosity:

$$\tau = \mu \frac{\partial U_i}{\partial x_j}$$

$$(7.1)$$

where τ is the shear stress $[N\ m^{-2}]$ and μ is the dynamic viscosity $[kg\ m^{-1}\ s^{-1}]$. Newton's law of viscosity states a linear relationship between shear rates and shear stresses, where μ does not vary with the deformation rate or time.

Many fluids do however not follow equation (7.1) and are thus non-Newtonian.

The rheology of the incoming sludge can be described by the Krieger model. The model relates the dynamic viscosity with the dispersed solid concentration using the following function:

$$\mu = \mu_c \left(1 - \frac{\phi_d}{\phi_{max}}\right)^{-\eta \phi_{max} \mu^*}$$

$$(7.2)$$

In this case, the relation can be considered as a model equation for the prediction of the effective viscosity of suspensions with monodispersed spheres that characterize the dispersed phase. In this study have been set $\eta = 2.5$, ϕ_{max} is the maximum

packing limit which has default value for suspended solids equals to 0.62, ϕ_d is chosen as the minimum between the ϕ_d value and $0,999\phi_{max}$ to prevent numeric indivergence phenomena, in the end, μ^* is set equal to 1 for solids particles.

Note that the Krieger relation exhibits correct limit behaviour of the studied system. The relative viscosity of the studied system, due to the Krieger relation shown above, goes to 1 when $\phi_d \to 0$, therefore, this case is known as Newtonian condition where just the continuous phase is considered.

7.5   Froude Densiometric Number

Based on the Einlaufbauwerke von Nachlärbecken report, it is possible to reduce the suspended solids at the outlet and thus improve the efficiency of the tank by changing the deflector radius and the cap dimension at the base of the deflector. Moreover, Krebs, (1991) shows that the energy flow becomes minimal if the Densiometric Froude number (FD) in the inlet section, takes on the unit value. Froude's number is defined as follows:

$$FD = \frac{u}{\sqrt{\frac{\rho_0 - \rho}{\rho} g\, h_i}}$$

(7.3)

Where u is the sludge velocity at the connection between the inner and the outer part of deflector with height equals to h_i. Knowing the inlet flow value, the velocity can be computed as:

$$u = \frac{Q}{2\pi\, r_i\, h_i}$$

(7.4)

Where r_i is the deflector radius (Fig. 7.2.a). Using the design values (Fig. 7.2.b-c) a Froude number of 0.21 is obtained. In order to get the Froude number equal to 1, the geometry parameters r_i e h_i can be modified. With the respect to the design project geometry (Fig. 7.2.c), it has been launched a first simulation with a $r_i = 0.60\ m$ and an $h_i = 0.18\ m$ (Fig. 7.2.d) and a second simulation using $r_i = 1.765\ m$ and $h_i = 0.09\ m$ (Fig. 7.2.e).
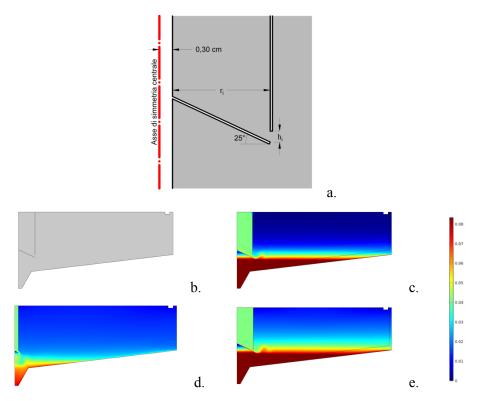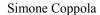
Fig. 7.2 – a. Deflector geometric scheme. b. Transversal section referement: c. Settler with a deflector radius r_i=1.765 m and height h_i=0.25 m; d. Settler with a deflector radius r_i=0.60 m and height h_i=0.18 m; e. Settler with a deflector radius r_i=1.765 m and height h=0.09 m

7.6 Results

The simulation results have been obtained by a time dependent simulation using 12 hours, time window. The simulation time was set long enough in order to allow the dispersed phase concentration, for the clarified and for the recirculated outlet flows, to reach a constant asymptotic value (as shown in Fig. 7.3). At the last time step simulation, the fluid pattern velocity become stationary.
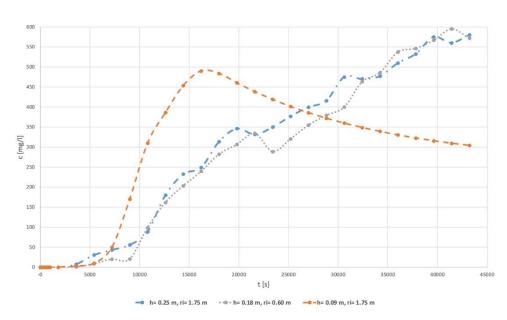
Fig. 7.3 – Trend concentration of dispersed solids at the clarified outlet

In the Fig. 7.3 are depicted the concentration curves of the dispersed solids at the clarified outlet. On y-axis the concentration is expressed in mg/l while on the x-axis the time in seconds. The blue curve shows the value of the designed settler, the orange and grey curves are related to the cases in the Fig. 7.2.d and Fig. 7.2.e based on the value of FD=1. Can be highlighted how the concentration of the case Fig. 7.2.e has a big drop in the outlet concentration.

The depicted graph gives a comparison between the results of the designed and the two studied cases. As a conclusion it has been obtained that the clarified concentration outlet of the case "e" is lower with respect the clarified concentration outlet of the designed project.

Using a FEM scheme, it has been provided that the use of the densiometric Froude number results a good tool for the design of deflectors and secondary settler.

7.7 Conclusion

A secondary settler intended for sugar waste treatment was numerically analized. The Densiometric Froude number (FD) was proven to be a suitable parameter for sizing the deflector system. During the design phase the FD can be adopted as a sizing parameter, but since the results can vary greatly, a CFD study was necessary to assess its influence, varying the geometry. Changing the diameter of the deflector

and the bottom opening allows to obtain lower Suspended Solids concentrations at the output of the secondary settler.

8. Oxygenation tank

8.1 Introduction

One of the targets in wastewater treatment field is guarantee the treatment processes efficiency and, at the same time, contain investment and operating costs. In order to optimize the energy consumption, the outflow quality should be aligned with the local technical standard

All the wastewater treatment plants need a bioreactor (Metcalf et al, 2003) but it, usually, has a large energy request with the consequent increase of the management costs.

The reactor uses the air to ensure the biochemical oxygen demand (BOD), furthermore, allows the suspension of the aerobic bacteria to ensure the reduction process of the suspended organic solids. To guarantee the bacteria suspension and the oxygen demand, the aeration unit needs a large energy consumption to activate the pumps that are always on work.

In this paper it will be assessed if can be guaranteed a good bacteria and oxygen diffusion in the aeration tank using a lower energy consumption by activating the pump intermittently.

One of the widely studied topic of the wastewater treatment automation is the regulation of the air flow inlet in the oxidation tank. The air flows are generally calculated with respect to the maximum designed flow in order to ensure the functionality of the tank even during the peak flow inlet. Instead, in case of lower inlet flow can be registered a lower request of pumped air to maintain the oxygenation in the tank. This will cause a lower efficiency of the tank in terms electrical usage for the air pumps than required.

For this reason, the aim of the research is to study the tank with a different inlet air flow, based on the air quantity necessary to provide a good oxygenation and suspended solids in the tank.

The Computational Fluid Dynamics simulations are largely diffuse to understand the fluids pattern in different wastewater treatment units.

8.2 Study Case

The study is composed of two parts, in the first it has been created an anoxic chamber to remove the nitrate. Two mechanic propellers provide the sludge mixing in order to avoid the sedimentation of the suspended solids. A map of the tank's geometry

can be observed in **Errore. L'origine riferimento non è stata trovata.**, where the mixer impeller and the air diffusers are shown.

The CFD model treated in the study does not take in to account the anoxic chamber, instead is focused on the effect of the air on the sludge in the aeration zone. The two parts are hydraulically connected by four slots of 1.5x1 m on the tank bottom.

The described units is the aeration tank of Oulx (Tourin, Italy) wastewater treatment plant with dimensions 22.5x14 m and a maximum wastewater level of 6 m. Inlet flow rate is set to 190 m^3/h. In the aeration zone are installed 338 circular nozzles with a diameter of 9 inch (0.23 m) positioned at a height of 0.28 m from the bottom of the tank.

The inlet air flow rate at each nozzle is 3.06 $N\,m^3/h$ whereas totally are issued 1034.28 $N\,m^3/h$ for the overall tank. Considering the sludge pressure on the nozzles, 60% relative humidity and the injected air temperature of 20°C, the effective air flow rate that for a nozzle of 1.62 m^3/h and for the overall tank of 547.56 m^3/h are derived by applying the state equation of perfect gas for simplicity.
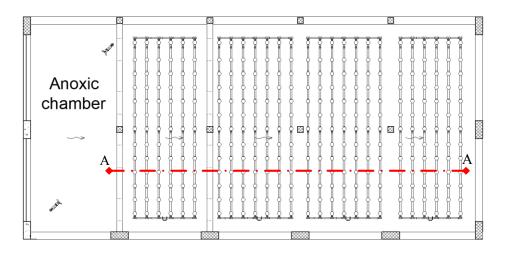

Fig. 8.1 – Tank top view

8.3   Numerical modelling

8.3.1   Domain

The geometry of the numerical modelling is a full scale 2D section (see **Errore. L'origine riferimento non è stata trovata.**) of the plant to alleviate the high computational cost for a full 3D simulation. In order to represent a simplified model

of the tank, the 2D model is obtained by exploiting the properties of symmetry of the tank's geometry. In this way all the process involved can be obtained at a lower computational cost. This section is considered as representative of the overall oxygenation tank. This approximation introduces some limits because the nozzles ended up being rectangular whereas they have a circular shape.

In the end the section includes all the nozzles in line with the others.

The tank is composed by three chambers, separated by a partition wall which allows the transition of the sludge among the chambers. The first chamber is the anoxic zone where a mechanical mixing starts the process. For this study are considered only the second and third zones where the aeration take place.

The simulation domain is meshed in 11251 elements, as shown in the Fig. 8.2 **Errore. L'origine riferimento non è stata trovata.**. In this domain the fluid patterns and the dispersed phase concentration are calculated. The nozzle geometry is amplified in **Errore. L'origine riferimento non è stata trovata.**.
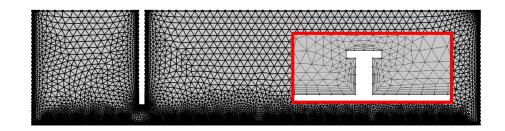

Fig. 8.2 – Mesh and nozzle's detail

8.4   Equations

Due to the high computational cost of a DNS simulation the k-ε model has been applied.

COMSOL Multiphysics has been used for this problem, adopting the mixture model to represent the fluid-particle interaction as a unique flow with average flow properties. It has been used a biphasic model made of a continuous phase, represented by the sludge, and a dispersed phase, represented by the air. The air flow is made of bubbles with a diameter range of $1 - 3$ mm, for this reason the fluid it was considered as an equivalent fluid. In this study has been set a medium and constant diameter of 2 mm for the bubbles.

The turbulent k-ε Model for mixture model is valid on the assumption that the density of each phase is approximately constant, both phases present equal pressure field and the particle relaxation time is short compared to the time-scales of the flow. In the two-phases model the disperse phase is treated as a second continuous phase interacting with the continuous phase where the conservation equations of mass (Eq. 4.1) and momentum (Eq. 4.2), the transport equations of turbulent kinetic energy (Eq. 4.3) and dissipation rate of turbulent kinetic energy (Eq. 4.6) are solved for the two fluid flows and are used interaction terms between the two flows.

Consequently, in order to separate the two phases, a transport equation for the dispersed phase volume fraction has to be added. This equation represents the variation in the time of the dispersed phase distribution, valid for the gas dispersed phases (Eq. 4.24)

Turbulence effects are modelled using the standard two-equation k-ε model for each phase. The k-ε Model uses two additional transport equations to describe the transport of turbulent kinetic energy k and turbulent dissipation rate ε. Kinetic energy k is "extracted" from the mean flow, by mean velocity gradients, and then transferred through the inertial range to the smallest scale, Kolmogorov scale, where viscous forces are comparable with inertial one and it is dissipated by ε

The drag forces are modelled by the Schiller-Naumann model for spherical particles (Schiller & Naumann, 1935).

During the aerobic phase the bacteria present in the tank, use oxygen to reduce the dissolved substances. In the oxygenation tank is injected the air with an oxygen concentration of 20%. For this reason, the nozzles air flow rate is calculated with respect to the oxygen demand and then sized with respect the oxygen percentage concentration. The process of oxygen consumption is considered homogeneous in the tank that is simulated by the mass transfer law. This assumption is valid only if all the bacteria are homogeneously suspended in the fluid, the oxygen mass transfer modelling requires the evaluation of the mass transfer coefficient, K_La. In this case it has been calculated that the oxygen consumption is equal to 5.14E-5 kg/(m³·s).

8.5   Results

In the simplified 2D aerated tank has been simulated three different scenarios to understand the air saturation time in the tank. The first has been calculated to obtain the maximum air fraction in the tank. The second one has been conducted with nozzles turned off obtaining the air outlet time range. The third one is a combination of the previous two.

With the first simulation it has been calculated the time needed to gain maximum air saturation and a stationary hydrodynamic condition. Both scenarios are displayed in the figures below where can be observed velocity variation up to 200 s step time. After that time step the velocity patterns are almost constant and, as it is shown in the Fig. 8.3, the average concentration curve became constant.
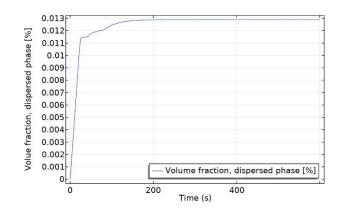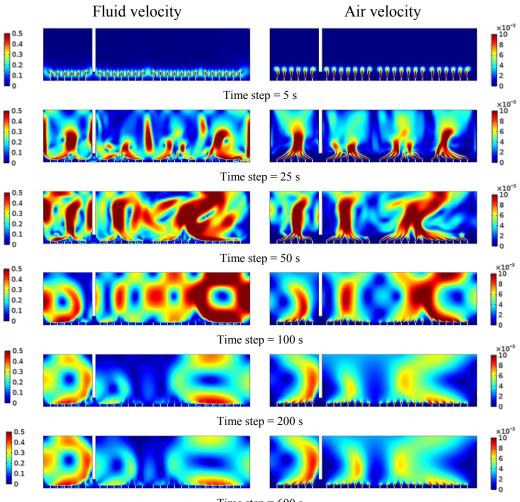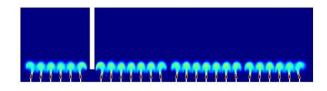

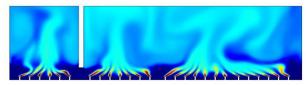*Fig. 8.3 – Dispersed phase volume fraction average in the first simulation*
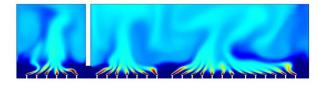
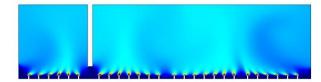*Fig. 8.4 – Fluid and air velocity field in different time step*
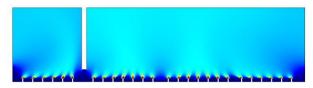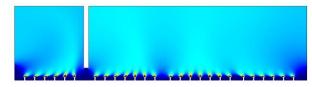
Time step = 5 s

Time step = 25s

Time step = 50s

Time step = 100 s

Time step = 200 s

Time step = 600 s

Fig. 8.5 – Dispersed concentration in different time step

The second simulation has been carried out with the nozzles off starting from the fluid and concentration pattern of the first simulation, at time step 200 s. The results of this simulation are the outflow time and the consumption time of the air flow. This interval is around 40 s, which corresponds to the shutting time of the nozzle pumps, avoiding the neutralization of the air concentration in the tank.

The total interval is 240 s

The time range of 240 s therefore provides a nozzles operating time of 200 s and a power-off interval of 40s. This definition allows us to realize a continuous simulation consisting of a sequence of intervals of 240 s.

In the third simulation the interval is repeated three times. The following diagram shows the average concentration in the tank with intermittency operations of the nozzles for a total time of 720 s.

Fig. 8.6 – Dispersed phase volume fraction average in the final simulation

The peaks are representative of the stationary condition in the tank and with initial condition of no air inflow. The Fig. 8.6 shows how the maximum average concentration value tends to constant values. Minimum values, have similar behaviour.

The fluid pattern of the simulation thus obtained, has been used to check whether the velocity field allows to keep the suspended solids in suspension inside the tank or whether they settle in the extinguishing interval. Particle tracking was used to carry out this study.

8.6 Conclusion

In this study an aeration tank was analysed by modifying the nozzles air flow, considering an intermittent operation system rather than a continuous operation system. The first step was to obtained the time range to achieve a constant air concentration, then after turning off the nozzles was registered a minimum air concentration. The exact time range was obtained by intermediate simulations to study the leakage and consumption time of the air with turned off nozzles. Once the operating cycles were determined, was registered an energy saving of 10% with respect the energy consumption required for a continuous operating system.

The suspended solids in the tank were studied using the particle tracking method that highlighted the beginning of a negligible sedimentation phase since it was due to some residual hydrodynamic activity.

9. Concluding remarks

Water scarcity is the main concern in many regions of the world. In facts, water accessibility of sufficient quality is becoming an increasingly serious problem, mainly due to the pollution of aquifers and coastal areas, climate change, and overpopulation. Therefore, an important part of the environmental degradation suffered by the planet is caused by the discharge of untreated or poorly treated wastewater.

Industrial, urban, and agricultural wastewater contain many different types of pollutants, these affect the human health. So, the current environmental situation of the planet requires that the selected treatment techniques must be adapted to their nature in order to optimize their removal. In addition to efficiency, wastewater treatment methods must be sustainable, not only from an environmental point of view, but also economically and ethically (Meliàn, 2020).

Therefore, the improvements of wastewater treatment plants include different aspects of water treatment such as the development of mathematical models, the experimental optimization of wastewater treatment methods and so on.

In this work, the feasibility and functionality of a modelling approach to decrease the Energy consumption and improve the efficiency of the processes in some Wastewater Treatment Plant units was assessed. The first step for each case was to find a literature support in order to understand the state of the research and identify eventually the critical points.

From the chapter 5 to 8 the main topic is the improvement of the treated units efficiency:

- In the chapter 5 (Anaerobic digester) two different mixing systems were analysed. As result the preferable is Gas mixing rather than the mechanical mixing, in terms of mixing efficiency and energy consumption. Indeed, the maximum velocity of the sludge was about three times larger than the one associated to the mechanical mixing systems; Furthermore, the dead zone percentage was one order of magnitude lower (about 5% against 50%);

- In chapter 6, the critical regions of a disinfection tank were identified, comparing on site measurements with the simulation model outputs. Indeed, the slow velocity areas correspond to the sections of the tank with a high PPA concentration. Consequently, non-homogeneous PPA mixing in the tank was observed.

   To solve the problem of the high concentrations in the "slow velocity" area, internal septa could be designed within the tank creating an established path for the water. This might promote the reaction between acid and water as the

increase of the contact time. In addition, there is a considerable energy saving as the impeller would no longer be necessary.

- In the chapter 7 (sedimentation tank) the efficiency of the secondary settler varying its geometry was assessed. The FD definition allowed a geometry variation of the secondary settler consistently. The geometry optimization, obtained by varying the deflector diameter and the bottom opening, decrease the suspended solids in the clarified outlet.

  It is shown that the FD Number can be a good parameter to design the deflector of the secondary settler. However, the use of the FD number does not guarantee an efficiency improvement, for this reason is preferable to combine it with a mathematical model. The combination of the FD and CFD allows to verify the results avoiding extra time and costs for the experiments on site.

- In chapter 8, the oxygen distribution and outlet time in order to determine the pumps operating interval was assessed. The obtained pumps shutting time is 40 seconds on an operating interval of 240 s. Turning off the pump 40 s each cycle gives an estimated energy saving of 10%.

  However, the shutting time could affect the biological processes that take place in the tank. The oxygenation tanks are designed to promote aerobic processes, but the shutting time could decrease the oxygen concentration up to activate the anaerobic processes.

The common aspect of the above recalled studies is the use CFD as a design/checking tool. Indeed, the use of CFD in WWT processes turned to be the most promising technology because can simulate complex processes bringing reliable results with low experimental costs. Still, there is no huge literature in the field of WWT.

In this study has been proven that the Computational fluid dynamics is a valuable and sometimes indispensable tool for designing new and retrofitting existing water and waste water systems. However, CFD models was used as a side exercise to complement the traditional design methods, mostly because of the culture of relying on proven methods in a traditional field, such has WWT.

10. References

Abuabdou, S. M., Ahmad, W., Aun, N., & Bashir,, M. (2020). A review of anaerobic membrane bioreactors (AnMBR) for the treatment of highly contaminated landfill leachate and biogas production: effectiveness, limitations and future perspectives. *Journal of Cleaner Production*, 255, 120215.

Abuabdou, S. M., Bashir, M., Aun, N., & Sethupathi, S. (2018). Applicability of anaerobic membrane bioreactors for landfill leachate treatment: review and opportunity. (p. 140 (1), 012033.). IOP Conference Series: Earth and Environmental Science.

Achkari-Begdouri, A., & Goodrich, P. (1992). Rheological properties of Moroccan dairy cattle manure. *Bioresource Technology*, 40, 149–156.

Amicarelli, A., Manenti, S., Albano, R., Agate, G., Paggi, M., Longoni, L., Pirovano, G. (2020). SPHERA v.9.0.0: a computational fluid dynamics research code, based on the smoothed particle hydrodynamics mesh- less method. *Computer Physics Communications*, 250, 107157.

Appels, L., Baeyens, J., Degrève, J., & Dewil, R. (2008). Principles and potential of anaerobic digestion of waste-activated sludge. *Progress in Energy and Combustion Science*, 34 (6), 755–781.

Armbruster, M., Krebs, P., & Rodi, W. (2001). Numerical modeling of dynamic sludge blanket behaviour in secondary clarifiers. *Water science and technology : a journal of the International Association on Water Pollution Research*, 43, 173-80.

Ayranci, I., Kresta, S., & Derksen, J. (2013). Experiments and Simulations on Bidisperse Solids Suspension in a Mixing Tank. *Chemical Engineering & Technology*, 36(11), 1957–1967.

Barnes, H. (2000). *A handbook of elementary rheology.* University of Wales Aberystwyth: The University of Wales Institute of Non-Newtonian Fluid Mechanics, Department of Mathematics.

Blais, B. (2016). Développement d'un modèle Euler-Lagrange robuste pour la simulation des écoulements solide-liquide dans les opérations de mélange. École Polytechnique de Montréal.

Blocken, B., & Gualtieri, C. (2012). Ten iterative steps for model development and evaluation applied to computational fluid dynamics for environmental fluid mechanics. *Environmental Modelling & Software*, 33 (7), 1–22.

Borole, A. P., Klasson, K., Ridenour, W., Holland, J., Karim, Z., & Al-Dahhan, M. (2006). Methane production in a 100-L upflow bioreactor by anaerobic digestion of farm waste. *Applied Biochemistry and Biotechnology*, 131 (1–3), 887–896.

Bouallagui, H., Marouani, L., & Hamdi, M. (2010). Performances comparison between laboratory and full-scale anaerobic digesters treating a mixture of primary and waste activated sludge. *Resources, Conservation and Recycling*, 55 (1), 29–33.

Bovolin, V., Viccione, G., Di Leo, A., & Dentale, F. (2017). A comparative numerical study of the coanda effect. *In: AIMETA 2017 - Proceedings of the 23rd Conference of the Italian Association of Theoretical and Applied Mechanics*, Vol. 2, pp. 1743–1753.

Chandran, J., Yogaraj, D., Manikandan, K., & Jeyaraman, P. (2017). Optimization of bio gas recirculation velocity in biogas mixing anaerobic digester with the feed of 8% TDS using CFD. *International Journal of Mechanical Engineering and Technology*, 8 (8), 596–606.

Dapelo, D. (2016). Gas Mixing in Anaerobic Digestion. *Ph.D. Thesis*.

Dapelo, D., & Bridgeman, J. (2018). Euler-lagrange computational fluid dynamics simulation of a full-scale unconfined anaerobic digester for wastewater sludge treatment. *Advances in Engineering Software*, 117, 153–169.

Dapelo, D., Alberini, F., & Bridgeman, J. (2015). Euler-Lagrange CFD modelling of unconfined gas mixing in anaerobic digestion. *Water Research*, 85, 497–511.

Derksen, J. J. (2003). Numerical simulation of solids suspension in a stirred tank. *IChE Journal*, 49(11), 2700–2714.

Ducoste, J., & Clark, M. (1998). The influence of tank size and impeller geometry on turbulent flocculation: I. Experimental. *Environmental Engineering Science*, 22 (5), 615–628.

Kariyama, I. D., Zhai, X., & Wu, B. (2018). Influence of mixing on anaerobic digestion efficiency in stirred tank digesters: a review. *Water Research*, 143, 503–517.

Krebs, P. (1991). The hydraulic of final settling tanks. *Water Science and Technology*, 23, 1037–1046.

Kushkevych, I., Cejnar, J., Vítězová, M., Vítěz, T., Dordevic´, D., & Bomble, Y. (2020). Occurrence of thermophilic microorganisms in different full scale biogas plants. *International Journal of Molecular Science*, 21 (1), 283.

Launder, B. E., & Spalding, D. (1974). The numerical computation of turbulent flows. *Computer Methods in Applied Mechanics and Engineering*, 3 (2), 269–289.

Leite, W., Magnus, B., Guimarães, L., Gottardo, M., & Belli Filho, P. (2017). Feasibility of thermophilic anaerobic processes for treating waste activated sludge under low HRT and intermittent mixing. *Journal of Environmental Management*, 201, 335–344.

Leonzio, G. (2018). Study of mixing system and geometric configurations for anaerobic digesters using CFD analysis. *Renewable Energy*, 123, 578–589.

Lin, H., Peng, W., Zhang, M., Chen, J., Hong, H., & Zhang, Y. (2013). A review on anaerobic membrane bioreactors: applications, membrane fouling and future perspectives. *Desalination*, 314, 169–188.

Lindmark, J., Thorin, E., Bel Fdhila, R., & Dahlquist, E. (2014). The effects of different mixing intensities during anaerobic digestion of the organic fraction of municipal solid waste. *Waste Management*, 34 (8), 1391–1397.

Lisowyj, M., & Wright, M. M. (2020). A review of biogas and an assessment of its economic impact and future role as a renewable energy source. *Reviews in Chemical Engineering*, 36 (3), 401–421.

López-Jiménez, P. A., Escudero-González, J., Montoya Martínez, T., Fajardo Montañana, V., & Gualtieri, C. (2015). Application of CFD methods to an anaerobic digester: the case of Ontinyent WWTP, Valencia, Spain. *Journal of Water Process Engineering*, 7, 131–140.

Manea, E., & Robescu, D. (2012). *Simulation of mechanical mixing in anaerobic digesters* (Vol. 74 (2), 235–242). UPB Scientific Bulletin.

Martin, T., Kamath, A., & Bihs, H. (2020). A Lagrangian approach for the coupled simulation of fixed net structures in a Eulerian fluid model. *Journal of Fluids and Structures*, vol. 94.

Martínez Mendoza, A., Montoya Martínez, T., Fajardo Montañana, V., & López Jiménez, P. (2011). Modeling flow inside an anaerobic digester by CFD techniques. *International Journal of Energy and Environment*, 2 (6), 963–974.

Meegoda, J. N., Li, B., Patel, K., & Wang, L. (2018). A review of the processes, parameters, and optimization of anaerobic digestion. *International Journal of Environmental Research and Public Health*, 15 (10), 2224.

Meister, M., Rezavand, M., Ebner, C., Pumpel, T., & Rauch, W. (2018). Mixing non-Newtonian flows in anaerobic digesters by impellers and pumped recirculation. *Advances in Engineering Software*, 115, 194–203.

Meliàn J.A.H. (2020). Sustainable Wastewater Treatment Systems. *Sustainability*, 12, 1940.

Meroney, R. N., & Colorado, P. (2009). CFD simulation of mechanical draft tube mixing in anaerobic digester tanks. *Water Research*, 43, 1040–1050.

Monteith, H. D., & Stephenson, J. (1981). Mixing efficiencies in full-scale anaerobic digesters by tracer methods. *Journal of the Water Pollution Control Federation*, 53 (1), 78–84.

Olsson, E., & Kreiss, G. (2005). A conservative level set method for two phase flow. *Journal of Computational Physics*, 210, 225–246.

Parker, D. S., Kaufman, W., & Jenkins, D. (1971). Physical conditioning of activated sludge flocs. *Journal Water Pollution Control Federation*, 43 (9), 1817–1834.

Parker, D. S., Kaufman, W., & Jenkins, D. (1972). Floc breakup in turbulent processes. *Journal of the Sanitary Engineering Division*, 98 (1), 79–99.

Pettersson Reif, B. A., & Durbin, P. (2001). *Statistical Theory and Modeling for Turbulent Flows.* Wiley.

Qasim, S. R. (1999). Wastewater Treatment Plants: Planning. Design and Operation.

Rendina, I., Viccione, G., & Cascini, L. (2019). Kinematics of flow mass movements on inclined surfaces. *Theoretical and Computational Fluid Dynamics*, 33 (2), 107–123.

Sadino-Riquelme, C., Hayes, R., Jeison, D., & Donoso-Bravo, A. (2018). Computational fluid dynamic (CFD) modelling in anaerobic digestion: general application and recent advances. *Reviews in Environmental Science and Technology*, 48 (1), 39–76.

Sajjadi, B., Raman, A., & Parthasarathy, R. (2016). Fluid dynamic analysis of non-Newtonian flow behavior of municipal sludge simulant in anaerobic digesters using submerged, recirculating jets. *Chemical Engineering Journal*, 298, 259–270.

Samstag, R. W., Ducoste, J. J., Griborio, A., Nopens, I., Batstone, D. J., Wicks, J. D., . . . Laurent, J. (2016). CFD for wastewater treatment: an overview. *Water Science & Technology*, 74 (3): 549–563.

Schiller, L., & Nauman, A. (1933). A drag coefficient correlation. *Verein Deutschen Ingenieure Zeitung*, 77, 318-320.

Seegmiller, H., & Driver, D. (1985). Features of a Reattaching Turbulent Shear Layer in Diverging Channel Flow. *AIAA Journal*, vol. 23, pp. 163–171.

Serna-Maza, A., Heaven, S., & Banks, C. J. (2017). In situ biogas stripping of ammonia from a digester using a gas mixing system. *Environmental Technology*, 38 (24), 3216–3224.

Shi, X.-S., Yu, J.-H., Yin, H., Hu, S.-M., & Huang, S.-X. (1995). Effect of Hydraulic Retention Time on Anaerobic Digestion of Wheat Straw in the Semicontinuous Continuous Stirred-Tank Reactors. *Computers & Fluids*, 24 (3), 227–238.

Sindall, R., Bridgeman, J., & Carliell-Marquet, C. (2013). Sindall, R., Bridgeman, J. & Carliell-Marquet, Velocity gradient as a tool to characterise the link between mixing and biogas production in anaerobic waste digesters. *Water Science & Technology*, 67 (12), 2800–2806.

Singh, B., Szamosi, Z., & Siménfalvi, Z. (2019). State of the art on mixing in an anaerobic digester: a review. 141, 922–936.

Singh, B., Szamosi, Z., & Siménfalvi, Z. (2020). Impact of mixing intensity and duration on biogas production in an anaerobic digester: a review. *Critical Reviews in Biotechnology*, 40, 508-521.

Stamou, A. (2008). Improving the hydraulic efficiency of water process tanks using CFD models. *Chemical Engineering and Processing: Process Intensification*, 47 (8), 1179-1189.

Stoppiello, M. G., Lofrano, G., Carotenuto, M., Viccione, G., Guarnaccia, C., & Cascini, L. (2020). A comparative assessment of analytical fate and transport models of organic contaminants in unsaturated soils. *Sustainability*, 12, 1–24, 2949.

Subramanian, B., Miot, A., Jones, B., Klibert, C., & Pagilla, K. (2015). A full-scale study of mixing and foaming in egg-shaped anaerobic digesters. *Bioresource Technology*, 192, 461–470.

Tang, J. (2009). *Comparison of Dairy Manure Anaerobic Digestion Performance in Gas-Lift and Bubble Column Digesters.* Blacksburg, VA, USA: Virginia Polytechnic Institute and State University.

Tchobanoglous, G., Stensel, H., Tsuchihashi, R., & Burton, F. (2014). *Wastewater Engineering: Treatment and Resource Recovery.* McGraw-Hill Education.

Terashima, M., Goel, R., Komatsu, K., Yasui, H., Takahashi, H., Li, Y., & Noike, T. (2009). CFD simulation of mixing in anaerobic digesters. *Bioresource Technology*, 100, 2228–2233.

Torotwa, I., & Ji, C. (2018). A study of the mixing performance of different impeller designs in stirred vessels using computational fluid dynamics. *Designs*, 2 (1), 10.

Tsuji, Y. (2007). Multi-scale modeling of dense phase gas–particle flow. *Chemical Engineering Science*, 62(13), 3410–3418.

Versteeg, H., & Malalasekera, W. (1995). An Introduction to Computational Fluid Dynamics: The Finite Volume Method. p. 198-203.

Vesvikar, M. S., & Al-Dahhn, M. (2005). Flow pattern visualization in a mimic anaerobic digester using CFD. *Biotechnology and Bioengineering*, 89, 719–732.

Viccione, G., Zarra, T., Giuliani, S., Naddeo, V., & Belgiorno, V. (2012). Performance study of e-nose measurement chamber for environmental odour monitoring. *Chemical Engineering Transactions*, 30, 109–114.

Wang, H., Larson, R., Borchardt, M., & Spencer, S. (2019). Effect of mixing duration on biogas production and methanogen distribution in an anaerobic digester. *Environmental Technology*, 93-99.

Wang, J., Xue, Q., Guo, T., Mei, Z., Long, E., Wen, Q., Huang, R. (2018). A review on CFD simulating method for biogas fermentation material fluid. . *Renewable and Sustainable Energy Reviews*, 97, 64–73.

Wicklein, E., Batstone, D., Ducoste, J., Laurent, J., Griborio, A., Wicks, J., Nopens, I. (2016). Good modelling practice in applying computational fluid dynamics for WWTP modelling. . *Water Sci. Technol.*, 73 (5), 969–982.

Wilcox, D. (1998). *Turbulence Modeling for CFD, 2nd ed.* DCW Industries.

Wu, B. (2010). CFD simulation of gas mixing in egg-shaped anaerobic digester. *Water Research*, 44, 1507–1519.

Wu, B. (2011). investigation of turbulence models for mechanical agitation of non-Newtonian fluids in anaerobic digesters. *Water Research*, 45 (5), 2082–2094.

Wu, B. (2012). Large eddy simulation of mechanical mixing in anaerobic digesters. *Biotechnology and Bioengineering*, 109 (3), 804–812.

Wu, B. (2014). CFD simulation of gas mixing in anaerobic digesters. *Computers and Electronics in Agriculture*, 109, 278–286.

Wu, B., & Chen, S. (2008). CFD simulation of non-Newtonian fluid flow in anaerobic digesters. *Biotechnology and Bioengineering*, 99, 700–711.

Zare, A. D., Saray, R., Mirmasoumi, S., & Bahlouli, K. (2019). Optimization strategies for mixing ratio of biogas and natural gas co-firing in a cogeneration of heat and power cycle. *Energy*, 181, 635–644.